Load Capacity of Low Speed Steel Wheels

B. van den Ende

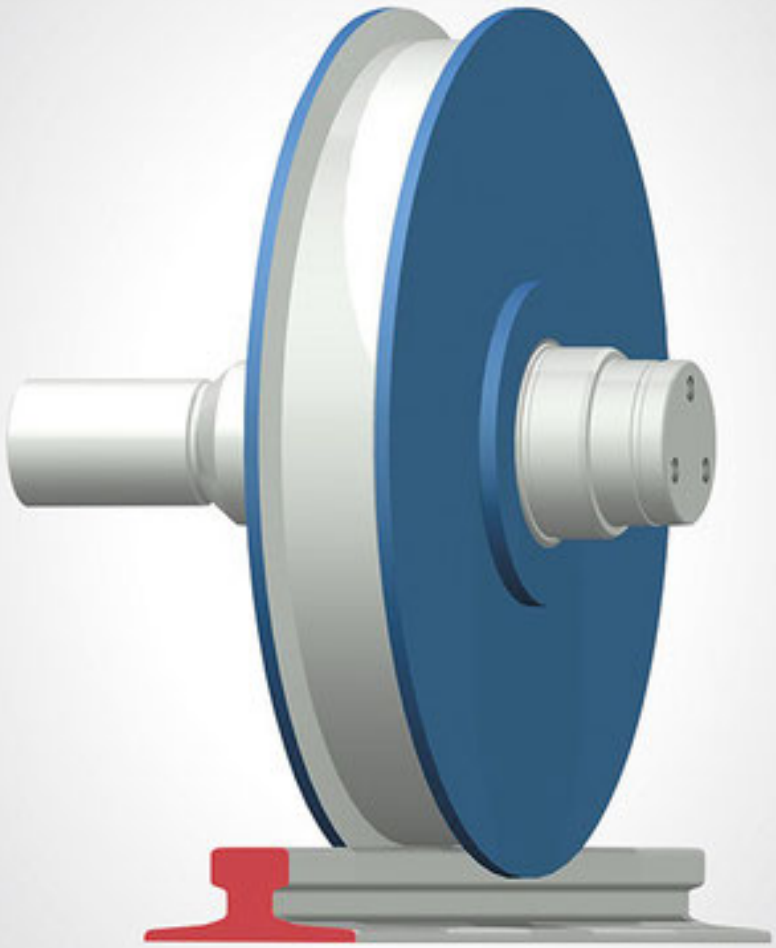

TU Delft

Load Capacity of Low Speed Steel Wheels

by

B. van den Ende

in partial fulfilment of the degree of Master of Science
at the Delft University of Technology.

Graduation project for the department MME

In collaboration with Huisman, Schiedam,
to be defended on Monday December 13, 2021.

Report number: **2021.MME.8569**

Student:	Bootsy van den Ende	4480678
Supervisor TU Delft:	Dr. C. L. Walters	
Supervisor Huisman:	Ir. M. Bloem	
Thesis committee:	Dr. ir. H. Polinder (chair) Dr. C. L. Walters Ir. M. Bloem Dr. ir. J. H. den Besten Prof. dr. Z. Li	

TU Delft

Preface

This thesis is a graduation assignment for completion of the MSc Mechanical Engineering, track Multi- Machine Engineering at the Delft University of technology. This projects aims to create a calculation method for calculating the lifetime of low speed steel wheels, and comparing this method to existing methods described by standards. This project is done in collaboration with Huisman, which uses many of these steel wheels in their equipment.

During completion of this project, many people from both the Delft University of Technology and Huisman have helped me with all problems that I had. First and foremost, I want to thank both of by supervisors, who have helped me almost every day over the past six months.

As my supervisor from the TU Delft, Dr. C. L. Walters helped me learn the fundamentals of Hertzian contact and fracture mechanics, and was always there when these theories became complicated. He provided me with enough knowledge to understand both these theories, and to apply them in this thesis. He also helped me to improve my knowledge by giving much positive feedback, thinking with me, and by connecting me with the right people. My daily supervisor at Huisman, Ir. M. Bloem, helped me to integrate in the company Huisman, which was a totally new experience for me. His experience with the company helped me to understand the problem that fatigue is for Huisman's equipment, and his explanation on the different software programs used was essential for me to understand these. His interest and in my project and the feedback helped me to create new knowledge for Huisman. I want to sincerely thank Dr. C. L. Walters and Ir. M. Bloem for everything they have done for me.

Furthermore, i want to thank Dr. E. Romeijn for helping me to formulate the project, and the feedback he gave me during our meetings. His knowledge about almost every aspect of this project gave me different perspectives on certain problems. I also would like to thank Prof.dr. Z. Li and Dr.ir. J.H. den Besten for our meetings, in which they used their expertise to help me with specific problems about the theories.

Due to the current COVID-19 Pandemic, it was not possible to meet many of the previously mentioned people face to face. However, due to great communication and many online meetings, this has not been a big problem for this project. Also, Huisman's great policy on working in the office, it was possible for me to work in office and have face to face contacts with my supervisor and others. I want to thank everybody for their effort and willingness to continue all the support online.

Finally, i would like to support everyone who has supported me the past 6 years. All the knowledge obtained during these years at TU Delft, and the continuous support of my friends and family made this project possible. I can not thank you enough.

Bootsy van den Ende
Delft, October 2021

Abstract

Steel wheels are often essential parts for heavy construction equipment, such as constructed by Huisman. These steel wheels must endure heavy loads. In order to prevent downtime, costs and to guarantee safety, it is important that the steel wheels do not fail. One important failure mode is failure resulting from subsurface initiated cracks. This research is focused calculating the allowable load for steel wheels with initial cracks as a function of the number of cycles.

The allowable load will be calculated using four different methods. Fracture mechanics will be applied, which uses an initial crack size and a load case to calculate the number of cycles until failure. The three other methods that will be discussed are described by fabrication standard, which are used during design of steel wheels. An analytical model will be used which applies all four methods to calculate the allowable load as a function of lifetime.

The results will be analyzed in order to understand the differences between the methods. Also, parametric research will be done in order to understand the effects of the fracture mechanics input parameters. Furthermore, experimental data will be used in order to estimate which method is most realistic. It can be concluded that fracture mechanics can be used to calculate the allowable load for steel wheels if the correct values for the input parameters are known. The acquired data is very limited, however, which indicates that more data must be gathered in order to specify the input parameters for specific situations and materials.

Nomenclature

ΔK	Stress intensity range	$MPa\sqrt{m}$
ΔK_{th}	Threshold stress intensity range	$MPa\sqrt{m}$
δ	Depth of diffusion (hardening depth)	mm
$\Delta\sigma$	Stress range	MPa
η	Location in y axis	mm
γ	Material parameter	$-$
γ_{cf}	General resistance coefficient	$-$
Ω	Contact surface area	mm^2
σ	Uni-axial stress	MPa
σ_1	Maximum principal normal stress	MPa
σ_2	Middle principal normal stress	MPa
σ_3	Minimum principal normal stress	MPa
σ_c	Compression stress	MPa
σ_m	Mean stress	MPa
σ_n	Normal stress component of stress σ	MPa
σ_s	Shear stress component of stress σ	MPa
σ_u	Ultimate strength of material	MPa
σ_x	Principle stress in x direction	MPa
σ_y	Principle stress in y direction	MPa
σ_y	Yield strength of the material	MPa
σ_z	Principle stress in z direction	MPa
$\sigma_{c,max}$	Maximum compression stress	MPa
$\sigma_{c,min}$	Minimum compression stress	MPa
σ_H	Stress under rolling contact	MPa
σ_{le}	Linear-elastic stresses for mode 1 fatigue	MPa
σ_{max}	Angle of maximum stress intensity	Rad
σ_{max}	Maximum stress value	MPa
σ_{min}	Minimum stress value	MPa
σ_{vm}	Von Mises stress	MPa
τ_{max}	Maximum shear stress	MPa

τse	Effective shear stress	MPa
θ	Angle between uni-axial stress σ and crack size direction a	rad
θ_o	Critical angle value	Rad
ξ	Location in x axis	mm
a	Crack length	mm
a_0	Initial crack size	mm
a_c	Critical crack size	mm
a_e	Major axis of contact ellipse	mm
A_f	Fatigue hardening factor	MPa
A_s	Static hardening factor	MPa
b	Crack height	mm
b_e	Minor axis of contact ellipse	mm
b_{eff}	Effective width of contact	mm
C	Intercept constant (Paris equation)	–
C	Total lifetime consumed (Miner's rule)	–
C_0	Intercept constant for $R = 0$	–
c_1	Fatigue factor for wheel rotation speed (FEM/ISO)	–
c_2	Fatigue factor for utilization and force spectrum (FEM/ISO)	–
C_d	Diffusivity constant	$mm/\sqrt{t^{1/2}}$
c_e	Effective contact radius	mm
D_1	Diameter of wheel	mm
D_2	Diameter of rail	mm
D_{eq}	Equivalent diameter of contact	mm
da/dN	Crack growth per cycle (crack growth rate)	$mm/cycle$
E	Elastic modulus	MPa
E'	Reduced elastic property	MPa
E_m	Equivalent elastic modulus	MPa
F	Load	N
f	Newman crack closure function	–
f_1	Edge pressure safety factor	–
f_2	Non-uniform pressure distribution safety factor	–
f_f	Factor of further influences	–
f_u	Reference force	N
f_{f1}	Edge pressure safety factor (equal to f_1	–

f_{f3}	Skewing factor	–
f_{f4}	Abrasion factor	–
$F_{fatigue}$	Allowed force for fatigue	N
F_{mean}	Average allowable load on wheel/rail for fatigue	N
F_{static}	Allowed static load	N
HB	Unit-Conform hardness (Brinell)	MPa
i_D	Rolling contact reference point	–
K	Stress intensity factor	$MPa\sqrt{m}$
k	Friction coefficient	–
K_c	Fracture toughness	$MPa\sqrt{m}$
k_c	Force spectrum factor	–
K_e	Elliptical ratio	–
k_h	Stribeck value	–
K_I	Mode I stress intensity factor	$MPa\sqrt{m}$
$K_{II,max}$	Maximum stress intensity factor for Mode II for all stresses σ	$MPa\sqrt{m}$
K_{II}	Mode II stress intensity factor	$MPa\sqrt{m}$
K_{max}	Maximum stress intensity (for σ_{max})	$MPa\sqrt{m}$
K_{min}	Minimum stress intensity (for σ_{min}	$MPa\sqrt{m}$
m	exponent for wheel/rail contacts	–
N	Current number of cycles	$cycles$
n	Material constant region II slope NASGRO equation and paris' law coefficient	–
$N(F_i)$	Allowed number of cycles until failure for current load case	–
N_f	Number of cycles until failure	$cycles$
n_i	Number of cycles for current load case (Miner's rule)	–
n_L	Total number of different load cases (Miner's rule)	–
N_{static}	Equivalent static rotations	–
p	Material constant region I tail NASGRO equation	–
P_L	Limiting pressure	MPa
P_{max}	Maximum pressure	MPa
P_{mean}	Mean pressure over surface	MPa
q	Material constant region III tail NASGRO equation	–
R	Stress ratio	–
r	Radius of rounded corners wheel/rail	mm
r_k	Crown radius wheel	mm

R_{1x}	Body 1 x-radius of curvature	mm
R_{1y}	Body 1 y-radius of curvature	mm
R_{2x}	Body 2 x-radius of curvature	mm
R_{2y}	Body 2 y-radius of curvature	mm
R_{eff}	Effective radius	mm
s_c	Force history parameter	–
u	Displacement	mm
u_z	Displacement in z direction	mm
v	Poisson ratio	–
v_c	Reference rolling contacts	–
w	total width of wheel or rail	mm
Y	Geometry factor	–
z	Depth in material	mm
σ_{c2}	Remaining compression stress in material depth	MPa

List of Figures

List of Tables

Contents

1 Introduction

1.1. Background

Huisman is a company that is specialized in designing and manufacturing heavy construction equipment [1]. It produces many different products, which all need to have specified loads in order to guarantee safety and to prevent failure. To make sure that this is true, knowledge about allowed load capacities is reflected in various design and fabrication standards. For structural and mechanical design, these standards serve as rules to measure or judge capacity [2]. The designed equipment needs to follow these rules, and has therefore a maximum safe load capacity.

1.2. Problem Definition

Many of Huisman's equipment types make use of steel wheels. Just like every specific part and equipment used in the industry, steel wheels also have design and fabrication standards which determine different values, such as the maximum safe load capacity. For steel wheels, one of the most important influences on the maximum safe load capacity is the cycle fatigue which occurs during usage of the wheels. Due to hundreds of years of steel wheel experience, mainly in railway systems, there is a lot of experience on steel wheels on steel rails at relatively high speed and with many revolutions, resulting in a relatively high cycle fatigue. Therefore, the current design and fabrication standards are mainly focused on high cycle fatigue. However, most of the steel wheels used by Huisman's products run at rather low speed with a relatively low amount of revolutions (between 1000 and 100.000 cycles), but with maximized loads. Although this is still considered mid to high cycle fatigue, the resulting allowed load described by different fabrication standards seem so have large differences for these relatively low numbers of cycles.

Therefore, Huisman would like to investigate fatigue of steel wheels, containing stress and lifetime calculations. This way, the highest reliable and safe load capacity of low speed steel wheels can be calculated according to a different method than the current fabrication standards, since these standards may not be accurate for the specified number of cycles. For these calculations, Fracture mechanics will be used. The results of this calculation will have to be compared to the existing standards in the form of an analytical model in order to clearly indicate the differences. If the standards seem to be inaccurate, it could potentially result in more safe, or more efficient equipment design and fabrication in terms of costs, time and weight.

In order to clarify the goal of this project, a research question is defined.

1.3. Research Goal

The research goal is defined in the form of a research question, which is defined as follows:

What is the maximum allowable load on steel wheels as a function of number of cycles used for a range between 10^3 *and* 10^7 *cycles? How do these values differ from the calculation standards and which method is most realistic?*

In order to answer this research question, different sub-questions are defined, which are:

1. How can the allowable load on steel wheels as a function of lifetime be calculated using fracture mechanics?
2. What are the methods currently used for calculating the maximum allowable load capacity according to the standards?
3. How do the results of the fracture mechanics calculations compare to the calculations using methods according to standards, and how to determine which method is most realistic?

1.4. Report Outline

The report is divided in different chapters in order to answer the previously defined sub-questions.

- **Chapter 2: Fatigue Calculations using Fracture Mechanics**
  Fatigue calculations on steel wheels will be done using Fracture mechanics. This method uses a stress intensity factor in order to calculate the lifetime dependent on material properties, initial parameters and the stress in the material resulting from the load contact. This contact between the wheel and the rail is analysed using the Hertz contact theory, which results in contact diameters and stress values, which can then be used in fracture mechanics calculations.
- **Chapter 3: Methods of Calculating the Load Capacity According to Fabrication Standards**
  There are many different fabrication standards which allow for load calculations on steel wheels. Three methods prescribed by the standards are used by Huisman, which are the FEM/ISO method, the EN method and the Horowitz method. For each of these methods, calculations for the static load, calculations for fatigue load related to lifetime, and calculations for desired hardening depth are explained, and their differences will be discussed.
- **Chapter 4: Analytical Model Results**
  Example calculations will be done using two different example wheels, which are real wheels used by Huisman. For both of these wheels, the maximum allowed load as a function of desired lifetime will be shown for all different calculation models. Also, the effect of the different input parameters used by the fracture mechanics method will be made clear using the model, since a number of values for these parameters is estimated, and the results are compared to experimental data.
- **Chapter 5: Conclusion and Recommendations**
  All information gathered in the previously discussed chapters will be used in order to answer the sub-questions stated before. This section will give an answer to these sub-questions, and the report will be concluded. Afterwards, recommendations will be made in order to continue and improve this research, since this project is only the tip of the iceberg.

1.5. Contribution

The contribution of this thesis will be a method of calculating the lifetime of high capacity steel wheels using fracture mechanics while implementing effects of friction between crack faces resulting from compression stresses. This model will be compared to existing methods described by fabrication standards, while also validating these results to experimental data in order to indicate which method is most realistic and why.

2

Fatigue Calculations using Fracture Mechanics

Rolling contact fatigue is currently considered the biggest failure mode for material deterioration. This chapter will focus on explaining how fatigue affects the lifetime of steel wheels by answering the first sub-question stated in the introduction:

How can the allowable load on steel wheels as a function of lifetime be calculated using fracture mechanics?

There are two main aspects of fatigue calculations on steel wheels which will be discussed in this chapter: The value of stresses resulting from the contact and the fracture mechanics which use these stresses to calculate crack growth and lifetime.
The interaction between wheel and rail, and how this has effect on the different stresses within the wheel and rail, will be explained using the Hertz contact theory, which will be explained in chapter 2.1. Chapter 2.2 will show the effects and causes of fatigue, and explain the fracture mechanics which enables calculation on fatigue lifetime. Afterwards, a short section will be dedicated to show what is meant by hardness and how surface hardening can improve the maximum allowable load.

2.1. Hertz Contact Theory

When bringing a steel wheel and rail into contact, the applied force will be transmitted over a contact area. This area is often small compared to the size of the wheel and rail. Wheel to rail contact can be divided in line or point contacts. When line contacts are subjected to a normal load, the resulting contact will be a strip shape contact [3]. When a point contact is subjected to a normal load, the resulting contact will be a circular or elliptical shape contact, depending on the relative curvature of the other surface, and the applied normal force. When analysing these contacts, the goal is to calculate the stresses and deformations of the contact and the interior of the bodies [4]. Most of the wheel and rail contacts result in elliptical shape contact. Traditionally, the Hertz theory of elliptic contact is used for calculating the pressure distribution in the contact.

2.1.1. Definition

The Hertz contact theory can be used using 5 important assumptions [5]:

- Ideally smooth and frictionless surfaces
- Identical material stiffness properties of both contacting bodies
- Linear elastic material (under certain loading conditions not valid in wheel–rail contact, but is a reasonable simplification, justified by the small amount of plastic material)
- Constant curvature of the bodies close to the contact area
- The extension of the contact area is small compared to body dimensions and radii

Although most of these assumptions can not always be completely true in reality, they are considered reasonable assumptions. The Hertzian approach dominates in simulations due to the simplicity.

The Hertz contact theory was the first theory that allowed for calculation on deformations, surface area and stresses occurring when two bodies come into contact. Since it is based on complicated mathematics, but results in a set of relatively simple equations, it is still the main theory used in simulation and calculation [4]. There are different types of contact surfaces: elliptical , spherical and cylindrical contact surfaces, of which the elliptical contact surface is the most common [6]. Since wheel/rail contact is considered a point contact, which results in a spherical or elliptical contact area when loaded, the focus will be on contact of ellipsoidal surfaces [3].

Wheel/rail contacts can be assumed as a contact between two ellipsoidal surfaces, which have orthogonal principal radii of curvature at contact location: R_{1x} and R_{1y} for body 1 and R_{2x} and R_{2y} for body 2.

2.1.2. Contact Area and Pressure Distribution

For the case of two ellipsoids in contact, the contact is described by the major (a_e) and the minor (b_e) axes of the contact ellipse, which are given by the following set of (approximate) equations [7]:

$$a_e = \alpha \sqrt[3]{\frac{3FR_{eff}}{E'}} \tag{2.1}$$

$$b_e = \beta \sqrt[3]{\frac{3FR_{eff}}{E'}} \tag{2.2}$$

Here, F is the load acting on the contact surface, and R_{eff} is the effective radius:

$$\frac{1}{R_{eff}} = \frac{1}{R_{1x}} + \frac{1}{R_{1y}} + \frac{1}{R_{2x}} + \frac{1}{R_{2y}} \tag{2.3}$$

$E^{'}$ is the reduced elastic property:

$$\frac{2}{E^{'}} = \frac{1-\nu_1^2}{E_1} + \frac{1-\nu_2^2}{E_2} \tag{2.4}$$

Where ν is the Poisson ratio. Many sources in literature use the reduced elastic property in a slightly different form. This can lead to confusion. However, since this form will be used in a different set of equations, it will result in the same values for contact dimensions and stress values as when using classical Hertzian equations given in textbooks.

α and β are defined as:

$$\alpha \approx \kappa^{\frac{1}{3}} \sqrt[3]{\frac{2E(m)}{\pi}} \tag{2.5}$$

$$\beta \approx \kappa^{-\frac{2}{3}} \sqrt[3]{\frac{2E(m)}{\pi}} \tag{2.6}$$

These functions themselves are approximated using:

$$E(m) \approx \frac{\pi}{2}(1-m)\left(1 + \frac{2m}{\pi(1-m)} - \frac{1}{8} ln(1-m)\right) \tag{2.7}$$

$$\kappa \approx \left(1 + \sqrt{\frac{ln(16/\lambda)}{2\lambda}} - \sqrt{ln(4)} + 0.16 ln(\lambda)\right)^{-1} \tag{2.8}$$

$$m = 1 - \kappa^2 \tag{2.9}$$

$$\lambda = \frac{R_x}{R_y}, 0 < \lambda < 1 \tag{2.10}$$

The mean pressure over the contact surface will then result in:

$$P_{mean} = \frac{F}{\pi a_e b_e} \tag{2.11}$$

And the maximum pressure, which is located at the center of the contact, will be:

$$P_{max} = \frac{3}{2} P_{mean} \tag{2.12}$$

The pressure at a certain point on the elliptical surface can be calculated using the following pressure distribution:

$$p(x,y) = P_{max}\sqrt{1 - \frac{x^2}{a_e^2} - \frac{y^2}{b_e^2}} \quad x \le a_e, y \le b_e \tag{2.13}$$

This distribution is, as said, highest at the center of the contact, as shown in figure 2.1.

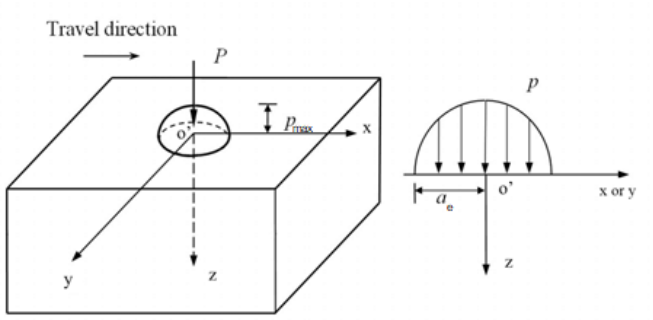

Figure 2.1: Pressure distribution

2.1.3. Surface Deformation

The pressure on the contact area as a result of the load deforms the material. Since the pressure is highest at the center of the contact, as shown before, the deformation is also highest at the center of the contact. However, the deformation at a specific location (x, y) in the contact area Ω is influenced not only by the pressure at that specific location, but by the pressure on the total contact area σ. Mathematically, integration of the deformation at point (x, y) caused by normal pressure $p(\xi, \eta)$ at point (ξ, η) over the entire area Ω will then calculate the total deformation at point (x, y). This results in the following equation for deformation due to the application of pressure p over surface area Ω. [6]:

$$u_z(x,y) = \frac{(1-\nu^2)}{\pi E} \iint_\Omega \frac{p(\xi,\eta)}{\sqrt{(x-\xi)^2 + (x-\eta)^2}} d\xi d\eta \tag{2.14}$$

For this purpose, ξ and η are chosen as coordinates in order to distinguish the location of deformation (x, y) from the integration of all locations (ξ, η) on the total contact area Ω. Figure 2.2 illustrates the deformation at point (x, y) as a result of the pressure p integrated over the surface area Ω. This equation is based on the assumption that the contact is frictionless. If this is not the case, the deformations will be in all three axis u_x, u_y and u_z, resulting in a more complicated set of equations, which can be found in [6]. Since the accelerations on most wheels used by Huisman are small, the contacts can be assumed frictionless. Therefore, acceleration effects will not be covered in this thesis.

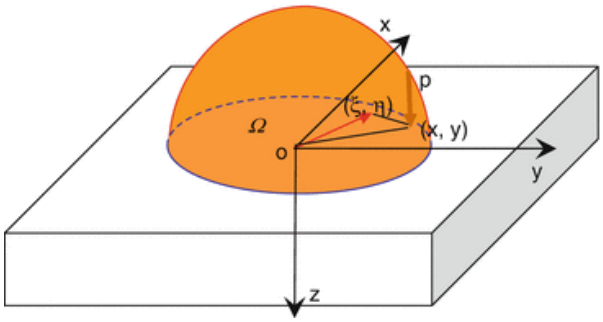

Figure 2.2: Deformation in point (x, y) as a result on the integrated pressure over Ω

2.1.4. Subsurface Stresses

The pressure caused by the load on the contact surface creates stress fields inside the material. These stresses can be explained using the maximum shear stress τ_{max}, and the von Mises stress σ_{vm} [8]:

$$\tau_{max} = \frac{(\sigma_x - \sigma_z)}{2} = \frac{(\sigma_y - \sigma_z)}{2} \tag{2.15}$$

$$\sigma_{vm} = \sqrt{\frac{(\sigma_x - \sigma_y)^2 + (\sigma_x - \sigma_z)^2 + (\sigma_y - \sigma_z)^2}{2}} \tag{2.16}$$

Here, σ_x, σ_y and σ_z are the principal normal stresses. The maximum for both the von Mises and Tresca stresses, and the depth at which they occur, are dependent on the elliptical ratio $K_e = b_e / a_e$ and the maximum pressure P_{max}, as shown by numerical solution in the table below.

Ellipticity	τ_{max}		σ_{VM}	
	Numerical solution		Numerical solution	
$K_e = b_e / a_e$	τ_{max} / P_{max}	at z/a_e=	σ_{VM} / P_{max}	at z/a_e=
0.20	0.321	0.149	0.586	0.142
0.40	0.325	0.266	0.605	0.260
0.60	0.322	0.355	0.615	0.355
0.80	0.316	0.425	0.619	0.425
1.00	0.310	0.480	0.620	0.480
1.25	0.316	0.531	0.619	0.531
1.67	0.322	0.592	0.615	0.591
2.50	0.325	0.665	0.605	0.650
5.00	0.321	0.745	0.586	0.708
Infinity	0.302	0.785	0.558	0.703

Table 2.1: Tresca and von Mises stresses depending on K_e [6]

The surface pressure due to the normal loads on the wheel/rail contact results in a three-dimensional stress distribution. The compressive stresses at the center of the contact are maximal at the surface of the wheel and rail, while the shear stress is maximum at a certain depth below the surface, which is shown in figure 2.3.

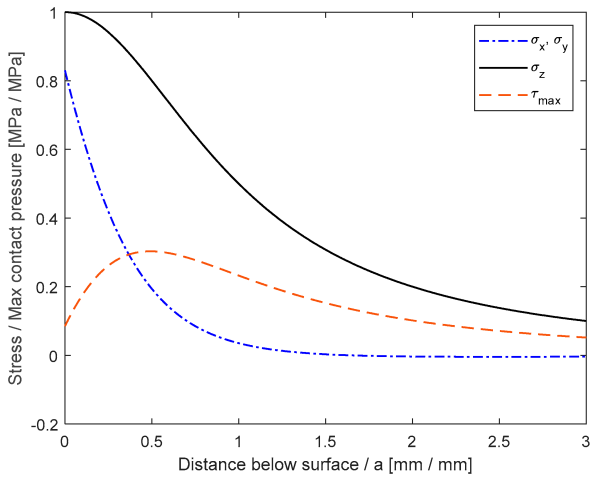

Figure 2.3: Three-dimensional stress distribution at center of contact [9]

The depth at which the maximum shear stress occurs is calculated differently for line or point contact cases. This is very important for determining the hardening depth, which will be explained in section 2.3. The point of maximal shear stress is the point in the material where yielding will start first, so the maximum allowable load must be calculated according to that location [3]. The described stress distribution is only valid for frictionless situations with only normal loading. If this is not the case, the stress field becomes distorted. The maximum shear stress depth is determined using figure 2.1.

2.2. Fatigue

Historically, wear was initially considered as the major cause of material deterioration. However, in today's world with improved gears, tracks, profiles, lubrication and better materials, wear is suppressed [10]. Currently, rolling contact fatigue, referred to as RCF, is considered the most important problem. Therefore, different methods of calculating fatigue have been developed, of which fracture mechanics will be used in this project.

2.2.1. Introduction to Fatigue

For wheel/rail contacts, surface initiated RCF cracks develop as a result of a frictional cyclic load which causes plastic flow of the material. These deformations will grow resulting in a crack-like flaw, which eventually results in an actual crack [11]. This crack will gradually grow due to cyclic loading, but also due to the effect of hydro-pressurisation caused by fluids being trapped in the crack [12] [13]. The cracks will further grow and can join together, as shown in figure 2.4.

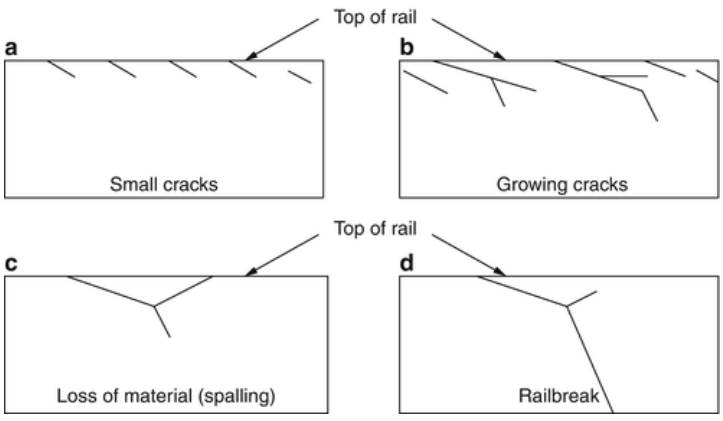

Figure 2.4: The different stages of RCF

This figure shows the different stages of RCF, where stage *a* represents the small initial cracks, stage *b* shows the further grow and joining of the cracks. After this, the cracks can propagate towards the surface, as shown in stage *c*. This can result in detachment of a part of the material, called spalling or pitting. If the cracks propagate deeper into the material, it will lead to rail or wheel break, which can cause serious accidents.

Besides surface initiated RCF, subsurface initiated RCF is another form of fatigue in wheel/rail contacts. This type of fatigue can be dangerous since it can not always be visually detected [10]. It initiates a crack at the depth with the highest shear stress and low material resistance. In a wheel, the crack will eventually grow towards the surface. It is important to realise that the initiation of subsurface initiated RFC is the combined effect of material defects and high loads. Therefore, material quality is of great importance to prevent this from happening. Just like surface initiated RCF, subsurface initiated RCF can result in spalling and total failure.

2.2.2. Stress Intensity Factor

Predicting fatigue is very difficult, since the initiation of cracks can happen in many different locations an have many different causes. Methods for fatigue analysis are often based on the relation between number of load cycles, stresses and loads. Analyzing fatigue crack growth will be done according to the concepts of fracture mechanics. Fracture mechanics uses a stress intensity factor K, which is a linear elastic parameter calculated as a function of applied stress, crack size and geometry. Failure occurs when the stress intensity factor K exceeds a critical value K_c of the material. It is useful for calculating crack growth rates as a function of crack size and stresses and is therefore a good method to calculate lifetime.

The stress intensity factor is also dependent on the Mode of fatigue. There are three primary modes of fatigue which define the orientation of crack relative to the loading, as shown in figure 2.5 [14] [15].

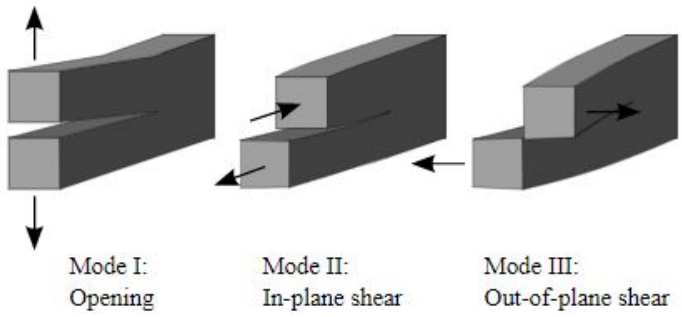

Figure 2.5: Three primary modes of fatigue [14]

Mode I is the result of a tensile stress pulling the crack faces apart, Mode II involves a shear stress in the direction parallel to the primary crack dimension, and Mode III is a shear stress perpendicular to the primary crack dimension. For engineering purposes, Mode I is almost exclusively considered for multiple reasons: Mode I is worst-case scenario and most common, and cracks that initiate in Mode II or Mode III will turn in Mode I situations as well. The linear-elastic stresses for Mode I fatigue in the direction of the applied loading can be calculated using the following equation:

$$\sigma_{le} = \sigma\sqrt{\frac{a}{2r}}cos\frac{\theta}{2}\left(1 + sin\frac{\theta}{2}sin\frac{3\theta}{2}\right) + ... \tag{2.17}$$

Here, a is defined as the crack size, and is half the length of the crack, as shown in figure 2.6. θ is defined as the angle between direction of crack size a, and the stress field σ, which in the case of figure 2.6 is 90°.

The stress intensity factor K is defined as:

$$K = \sigma\sqrt{\pi a} \tag{2.18}$$

Substitution, rewriting and the assumption that $\theta = 0$ results in the following simplification:

$$\sigma_{le} = \frac{K}{\sqrt{2\pi r}} \tag{2.19}$$

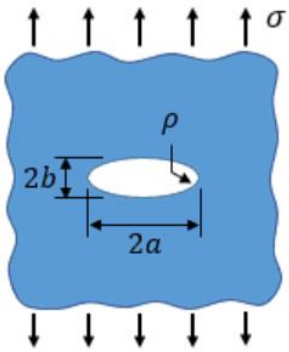

Figure 2.6: Dimensions of a crack

This equation is valid for ideally sharp crack tips. For situations with real crack geometries, the stress intensity factor can be generalized as:

$$K = Y\sigma\sqrt{\pi a} \tag{2.20}$$

Here, a is the crack size as explained before, and Y is the geometry factor which is dependent on the geometry of the crack, geometry of the part and the loading configuration [14]. This factor is the difficult part of calculating the stress intensity factor, but for many load cases, the solutions can be found in literature, such as [16]. When the stress intensity factor K is known, it can be used to calculate crack growth, and eventually predict the remaining lifetime. Using boundary conditions, the determination of the geometry factor can be simplified. According to [15], the geometry factor for Mode II can be approximated as $Y = 1$ for small cracks compared to a large component when shear stresses are applied, and [17] states that the geometry factor $Y = 1$ for a through centre crack with no separation. Since this research will focus on Mode II, which will be explained below, fatigue of relatively large wheels, and since cracks will have no separation due to compression states, both of these assumptions are good assumptions for this research, so the geometry factor will be assumed to be $Y = 1$. For a more detailed approximation of the geometry factor Y, FEM analysis of the specific situation can be done. It is important to realize that the geometry factor is only dependent on the crack geometry, and not on the angle. However. the angle does effect the combination between Mode I and Mode II. The effect of the angle returns in the equation for the stress intensity factor, as shown in equation 2.21 and 2.22. Other methods include the effects of the angle in the geometry factor, and can therefore differ from this method.

2.2.3. Different stresses

In order to use the stress intensity factor to make calculations on the lifetime of the wheel or rail, it is important to know the maximum value of the stress intensity at the crack tips. As shown before, there are two forms of rolling contact fatigue: Surface and subsurface initiated fatigue. The maximum stress intensity factors for both situations will be calculated using the equation for the stress intensity factor shown in equation 2.20, which will then be adjusted to account for the effects caused by the stress state. Afterwards, both situations will be compared in order to find the maximum value for the stress intensity factor.

Surface initiated fatigue

The maximum stress intensity factor occurring at the surface of the contact is calculated using the maximum pressure calculated using the Hertz contact theory. However, the general equation does not take the stress state and the effects of the angle of the crack compared to the surface into account. This general equation is considering tensile stresses an angle $\theta = 90°$, which is a crack parallel to the surface. If this angle is not 90°, the crack will also be subjected to shear stresses which relate to Mode II [18], which is illustrated in figure 2.7.

Therefore the stress intensity factor K is split up into respectively K_I, concerning Mode I, and K_{II}, concerning Mode II [17] [19]:

$$K_I = Y\sigma\sqrt{\pi a}\, sin^2(\theta) \tag{2.21}$$

$$K_{II} = Y\sigma\sqrt{\pi a}\, sin(\theta)\, cos(\theta) \tag{2.22}$$

When under compression stress σ_c instead of tensile stress, the crack will not open, but instead close. This

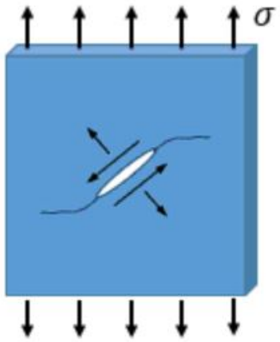

Figure 2.7: Different fatigue modes resulting in Mode I [14]

results in the disappearance of Mode I fatigue, and therefore the Mode I stress intensity factor. However, the material is still influenced by shear for which equation 2.22 is still valid. This equation, however, does not take frictional effects into account which are present due to compression. Since the crack is closed in compression, friction between crack faces indeed plays an important role. In order to account for the friction effect, the effective shear stress τ_{se} is introduced, which is defined as the subtraction of the frictional stress resulting from normal stress σ_n from the shear stress τ:

$$\tau_{se} = \tau - k\sigma_n = \sigma_c \, sin(\theta)\Big(cos(\theta) - k \, sin(\theta)\Big) \tag{2.23}$$

Here, k is the friction coefficient. An important value is the critical value for the angle θ, which is determined by [17]:

$$\theta_o = cot^{-1} k \tag{2.24}$$

This value is important since it is used to calculate the angle for maximum stress intensity factor for any given compression stress σ_c, which is $\theta_{max} = \theta_o/2$. Substitution results in an equation for the maximum stress intensity factor at the surface of the material:

$$K_{II,max} = Y\sigma_c\sqrt{\pi a}(1 - cos(\theta_{max}))/(2 \, sin(\theta_{max})) \tag{2.25}$$

Subsurface initiated fatigue
Subsurface initiated fatigue is initiated due to shear stresses induced in the material, which are the result of the normal stresses at the surface of the contact. The maximum value of this shear stress is defined in equation 2.15, and the value can be determined using the maximum contact pressure, as shown in figure 2.1. The stress intensity factor due to the shear stresses are:

$$K_{II} = Y\tau_{max}\sqrt{\pi a} \tag{2.26}$$

The angle of maximum shear stress can be determined using Mohr's Circle. It shows a clear relation between the principal normal stresses and the induced shear stress, and the angle between these stresses. The Diameter of the circle is the difference between the minimum and maximum principal normal stresses. Mohr's circle also shows that the value for maximum shear stress τ_{max} is equal to the radius of the circle, which is half of the diameter. This is consistent with equation 2.15.

For maximum shear stress, the angle 2θ must be 90°, which therefore results in a real angle θ of 45°. This means that the shear stress is maximum when the angle with respect to the normal stress is 45°.

The frictional effects have to be taken into account, as described in equation 2.23. However, the compression stress σ_c has a different value at a depth in the material then at the surface. Therefore, σ_{c2} is used. Rewriting results in the following equation for effective shear stress:

$$\tau_{se} = \tau_{max} - \sigma_{c2} * k \, sin^2(\theta) \tag{2.27}$$

According to figure 2.1, τ_{max} can be assumed to be approximately $0.32 * \sigma_c$, and the depth at which this occurs is dependent on the ellipticity of the contact. When the depth of highest shear stress is known, the value

of the normal stress σ_{c2} dependent on the depth z and the contact radius for spherical contacts can be calculated using [20]. Note that this is negative due to the defined positive direction in the coordinate system.

$$\sigma_{c2} = \frac{-P_{max}}{1 + \frac{z^2}{a_e^2}} \tag{2.28}$$

For elliptical contact, this results in:

$$\sigma_{c2} = \frac{-P_{max}}{1 + \frac{z^2}{c_e^2}} \tag{2.29}$$

with:

$$\frac{1}{c_e} = \frac{1}{a_e} + \frac{1}{b_e} \tag{2.30}$$

the depth of maximum shear stress z is approximated using the following equation, which is an curve fit to figure 2.1 [21]:

$$z \approx b_e\left(0.7929 - 0.3207\frac{a_e}{b_e}\right) \tag{2.31}$$

Comparison

All of the wheels and rails used by Huisman are made of steel, which have an estimated friction coefficient of $k = 0.78$, and the maximum shear stress according to figure 2.1 is approximately $\tau_{max} \approx 0.32 * \sigma_c$. Using these values, comparing the surface and subsurface initiated variants of the stress intensity factor shows that the subsurface stress intensity factor is higher then the stress intensity factor at the surface. According to this calculation, subsurface initiated rolling contact fatigue should be the main failure mechanism, which is indeed the case for most of Huisman's wheel and rail failures according to failure data.

2.2.4. Crack Growth

The crack size a grows as a function of the number of cycles N, where the growth rate is defined as da/dN, as shown in figure 2.8. The figure shows that the crack initially grows slowly, but the growth rate increases as crack size increases. The crack grows up to a critical size a_c with number of cycles N_f, at which failure will occur.

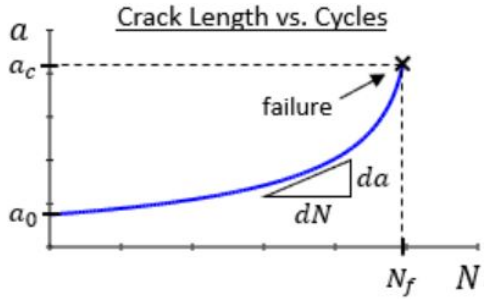

Figure 2.8: Crack Length vs. Cycles [22]

When a load is applied in a cyclic manner, this will result in maximum values and minimal values of applied stresses, respectively σ_{max} and σ_{min}. These values will be used to calculate:

Mean stress:

$$\sigma_m = \frac{\sigma_{max} + \sigma_{min}}{2} \tag{2.32}$$

Stress range:

$$\Delta\sigma = \sigma_{max} - \sigma_{min} \tag{2.33}$$

Stress ratio:

$$R = \frac{\sigma_{min}}{\sigma_{max}} \tag{2.34}$$

Since the stress intensity factor is linear with stress, as shown in equation 2.20, the values for mean stress, stress range and stress ratio for compression stress can be used to calculate:

Maximum stress intensity:

$$K_{II,max} = Y\tau_{se,max}\sqrt{\pi a} \tag{2.35}$$

Minimum stress intensity:

$$K_{II,min} = Y\tau_{se,min}\sqrt{\pi a} \tag{2.36}$$

Stress intensity range:

$$\Delta K = K_{max} - K_{min} \tag{2.37}$$

Stress intensity ratio (same as equation 2.34):

$$R = \frac{K_{min}}{K_{max}} \tag{2.38}$$

Simply stated: a fluctuating stress with range $\Delta\sigma$ results in a fluctuating stress intensity with range ΔK. When this stress range ΔK is applied to a material for a number of cycles ΔN, the crack will grow in length with Δa. The resulting growth rate of the crack will then be $\Delta a/\Delta N$, or in continuous form: da/dN.

When the growth rate of the crack da/dN, and the stress intensity range ΔK are plotted on a log-log scale, the graph typically take the form shown in figure 2.9. This figure clearly indicates three regions. region II

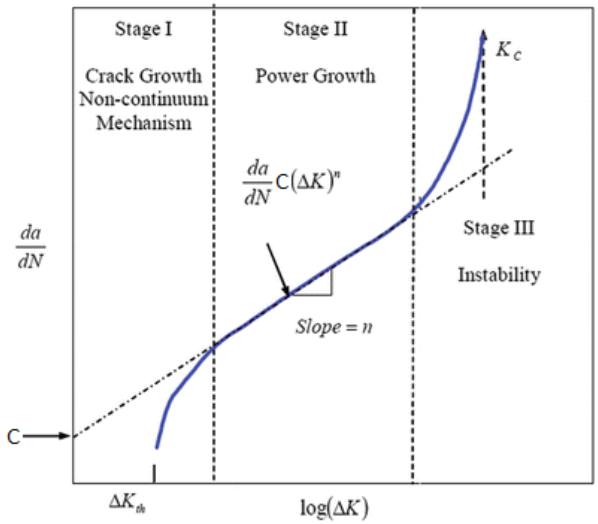

Figure 2.9: Crack growth rate da/dN vs stress intensity range ΔK [23]

is a straight-line region described by a curve called the Paris curve [22][24], which will be discussed below. Regions I and III are the upper and lower end tails which approach vertical asymptotes. The tail in region I approaches the fatigue crack growth threshold. stress intensity ranges below this value typically do not generate crack growth. The tail in region III shows accelerating crack growth. Cracks in this region grow rapid and unstable, and will eventually result in failure.

Crack growth can be described using a set of combined equations, starting with the Paris equation [24], which describes the straight-line region (region II):

$$\frac{da}{dN} = C(\Delta K)^n \tag{2.39}$$

Here, C is the intercept constant, and n is the slope on log-log scale, as visualized in figure 2.9. Both values for C and n can be found in literature or by testing. Values for n can range between 2 to 8 or 9 [25]. According to the British Standards BS 79010, the parameter n can vary, but can be roughly assumed: $n = 3$ [26]. It is important to realize that this equation does not account for the effects of stress ratio R. However, the

stress ratio R does have effect on the growth rate. Therefore, the Walker equation can be used, which is a generalization of the Paris equation to account for the effects of R:

$$\frac{da}{dN} = C_0\Big(\frac{1}{(1-R)^{1-\gamma}} * \Delta K\Big)^n \tag{2.40}$$

Where:

- R is the stress ratio, as defined in 2.34. High values of R result in higher values of crack growth rate.
- C_0 is the intercept constant C for the case when $R = 0$, which for steels in open air environments is recommended by the British standards BS 7910 to be $5.21 * 10^{-13}$ [26] [27].
- γ is a material coefficient which indicates how strongly the stress ratio R affects the growth rate. High values of γ decrease the effect of R.

The Walker equation does not take the lower and upper tail (region II and III) into account. Therefore, the NASGRO equation is used. The NASGRO equation accounts for stress ratio R, the lower and upper tail, and crack closure effects:

$$\frac{da}{dN} = C_0\Big[\Big(\frac{1-f}{1-R}\Big)\Delta K\Big]^n \frac{\Big(1-\frac{\Delta K_{th}}{\Delta K}\Big)^p}{\Big(1-\frac{K_{max}}{K_c}\Big)^q} \tag{2.41}$$

Where:

- ΔK_{th} is the threshold stress intensity range. as shown in figure 2.9. When $\Delta K \leq \Delta K_{th}$, da/dN can be assumed 0 [26].
- K_c is the fracture toughness of the material
- f is the Newman crack closure function
- p and q are material coefficients that describe the curvature of the tail sections, and can be obtained via literature or experimental data [22] [28].

Most of these parameters can be determined using different methods and approaches, and create complicated analytical solutions, which are described in literature as for example [29] and [30]. Since this does not focus on life prediction calculations, and shis equation is hardly validated for Mode II, this will be considered out of the scope of this project. The fracture toughness of the material K_c is, however, of much importance for calculating the life prediction of the material. Besides its presence in the NASGRO equation, the fracture toughness will be used in life prediction in section 2.2.5. It is defined as the point at which the crack growth rate will enter region III, as shown in figure 2.9. From this point, the crack will grow uncontrolled and will grow rapidly until it reaches the surface of the material. The part is therefore considered failed when K_{max} is higher then K_c. Although considered failed, is does not necessarily mean that the part in question is practically failing. This is dependent on the loading conditions of the part, and the location and orientation of the crack.

2.2.5. Life Prediction

In order to predict the lifetime of a cracked part, an initial condition must be known, which expresses the expected initial crack size a_0, the minimum and maximum stresses σ_{min} and σ_{max}, and the step size for number of cycles ΔN. The initial crack size a_0 is the maximum original defect size of the material at the beginning of its lifetime, tested with nondestructive testing. If the initial crack size is smaller then the sensitivity of the measuring equipment, the crack size can not be detected, and is therefore assumed to be the size of the measurement sensitivity [31] [14]. If experimental data is available, this can be used for calibration.

The following steps are used to calculate the lifetime of a cracked part with minimized initial cracks:

1. Calculate the maximum stress intensity factor for the current crack length:

$$K_{II,max} = Y\tau_{se,max}\sqrt{\pi a}$$

2. Check if the maximum stress intensity exceeds the material's fracture toughness: is $K_{max} \geq K_c$? If yes, the simulation is stopped and the part is considered failed. If not, the simulation continues to the next step.

3. Calculate the stress range and stress intensity range:

$$\Delta\sigma_c = \sigma_{c,max} - \sigma_{c,min}$$

$$\Delta K = K_{max} - K_{min}$$

4. Use the calculated stress intensity range to calculate the crack growth rate da/dN according to one of the methods. For instance, for simplification the Walker equation can be used, or for more detailed results, the NASGRO equation can be applied.

5. Use the crack growth rate and the determined cycle step size to calculate the incremental growth of the crack:

$$\Delta a = \frac{da}{dN}\Delta N$$

6. Now, the new crack size can be calculated, and the current total number of cycles can be updated:

$$a_{i+1} = a_i + \Delta a \qquad N_{i+1} = N_i + \Delta N$$

7. Use the new crack size for the next iteration of the simulation, until the failure condition is met. At this point, the number of cycles until failure N_f is the current number of cycles N_i, and the critical crack size a_c is the current crack size a_i.

2.3. Hardening

Material hardness is a material property which enables it to resist plastic deformation [32]. It is the material property which enables it to resist permanent deformation when a load is applied. Due to the lack of definition, it may not be a fundamental property of a material, but rather a composition of different properties, such a the yield strength and the modulus of elasticity. This results in several different types of hardness definitions, of which the Brinell Hardness will be used in this thesis since Huisman designs equipment using various standards which use the "Unit-Conform hardness", which is based on the Brinell hardness. The Brinell hardness is determined by forcing a very hard sphere of a known diameter with specified load into the surface of the test material [32]. By measuring the diameter of the indentation after the test and converting this to a surface area, the Brinell hardness number van be obtained by dividing the load used by the surface area of the indentation. This measurement results in a value in N/mm^2, but the units are often not stated.

For steel wheels, the highest amount of shear stress stress is, as explained before, found at a certain depth beneath the surface of the wheel. In order to increase the strength of the wheel, surface hardening can be applied which hardens the surface of the wheel up to a certain depth. It is very important that this hardening depth is deeper then the depth of maximum shear stress in order to avoid crack development, which is illustrated in figure 2.10. The required depth will be covered and calculated according to fabrication standards in chapter 3. Using surface hardening, the wheel has a higher hardness at the locations where stresses are high, and the maximum load capacity of the wheel will increase. Surface hardening of steel is done by chemically modifying the surface of the material. Carbon diffuses into the surface of the steel at very high temperatures, which makes the material harder. Temperatures are usually between 925°C and 955°C [33]. The depth of the diffusion is time, temperature and material dependent:

$$\delta = C_d\sqrt{t} \tag{2.42}$$

Where:

- t is the time of diffusion
- C_d is the diffusivity constant, dependent on the temperature, chemical composition of the steel and the concentration gradient of the hardening element [34].

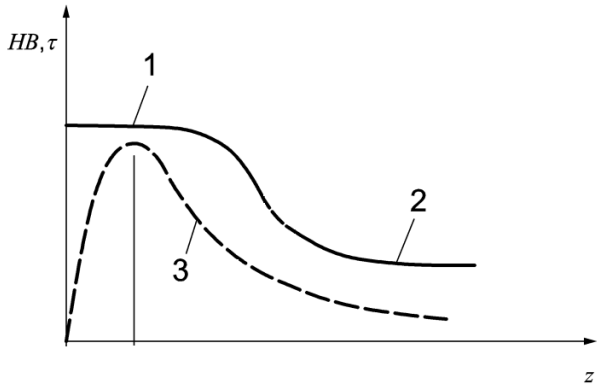

Figure 2.10: (1) surface hardness, (2) natural material hardness, (3) shear stress [35]

It is known that higher hardness values result in longer lifetimes for mechanical equipment. This is, however, not clearly shown in fracture mechanics. Literature does not show any correlation between crack growth rate and hardness. However, since practice shows a correlation between hardness and lifetime, it is expected that hardness and one, or maybe multiple, input parameters are correlated to hardness. Chapter 4 will include the effect of the different fracture mechanics input parameters on the allowable load, which will help identify the correlation between hardness and fracture mechanics.

3

Methods of Calculating the Load Capacity According to Fabrication Standards

Steel wheels have two main failure mechanisms: Static failure and Fatigue failure. Static failure occurs if a high force acts on the wheel, which makes the wheel deform and therefore fail. This failure mechanism only occurs if big calculation errors are made. Fatigue failure occurs if cracks have propagated to a critical size, which is caused by a non-critical force that is active for many wheel rotations or over rolls. Many different methods have been developed to calculate the maximum of these allowed forces together with the consumed lifetime and required hardness depth. This chapter will focus on explaining the important methods used by Huisman, and therefore answer the second sub-question stated in the introduction:

What are the methods currently used for calculating the maximum allowable load capacity according to the standards?

Recently, Huisman standards D00001439 addressing wheel and rail designs were in place [3]. These standards were for the most part derived empirically, which eventually resulted in problems. Therefore, Huisman now has a new approach based on generally accepted methods, of which the most important three are:

- FEM 1.001 b4 / ISO 16881-1, which is one method used by two standards
- EN 13001-3-3 standard, which is currently the preferred method used by Huisman
- Horowitz, which used to be the preferred method used by Huisman

Three main calculations will be shown per standard: Static load cases, Fatigue load cases, and the required hardness depth. Another important aspect concerning fatigue load cases is the lifetime of the wheel or rail. Fatigue load cases are dependent on a force and an amount of rotations that this force is active. To determine how much of the total lifetime of the wheel or rail is consumed by the load cases applied, Miner's rule is used:

$$C = \sum_{i=1}^{n_L} \frac{n_i}{N(F_i)} \tag{3.1}$$

Where:

- i is the current load case
- n_L is the total number of different load cases
- n_i is the number of rotations or over rolls for the current load case
- $N(F_i)$ is the allowed number of rotations or over rolls for the current load case. This value is calculated differently for each method.

The calculations described below have to be done for both the wheel and the rail separately since they can have different material properties and amount of rollings. Besides the different input parameters due to possibly different material, the calculations for wheel and rail are equal. It is important to determine when a part is considered "Failed". This is defined in EN 13001-3-3, and will be used for all methods. Wheel or rail has failed at a permanent radial deformation of 0.02% of the wheel radius. Although this has nothing to do with fatigue, is it the main failure criterion for the EN 13001-3-3
If the wheel or rail is to be hardened, it is important that this is done to the appropriate depth. This is because the maximum shear stress that occurs during a load case is not found at surface level, but in a certain depth. The different methods have different equations for determining this hardening depth, and will also be discussed in this chapter.

3.1. FEM 1.001 b4 / ISO 16881-1 [36] [37] [3]

FEM 1.001 b4 and ISO 16881-1 are two standards which describe the same method. Where the FEM 1.001 describes rules for designing hoisting appliances as a whole, ISO 16881 is mainly focusing on sizing iron or steel wheels and calculating the local stresses and uses equations described by ISO 16881. Advantages of using the FEM/ISO method are the fact that it uses straightforward formulas, uses limited number of inputs and it is suitable for both allowable stress and limit state method. Disadvantages, however, are that it offers a simplified approach due to a limited number of input parameters. Also, due to the formulation of the allowed fatigue force in discrete steps, there is no continuous formulation of the allowed rotations as a function of the force.

The FEM/ISO method is also limited. It can only be used if:

- The wheel diameter is below 1250 mm
- The ultimate strength of the wheel is above 500 N/mm^2

This can be a problem for Huisman applications, since many of Huisman's wheels have a larger diameter then 1250 mm.

3.1.1. Static Load Cases

For FEM/ISO, the allowed static force is given by the following equation:

$$F_{static} = 1.9 P_L b_{eff} D_{eq} \tag{3.2}$$

Where:

- b_{eff} is the effective width
- D_{eq} is the equivalent Diameter
- P_L is the limiting pressure

The effective width is the width of the contact between the wheel and the rail. For a situation where both wheel and rail have a flat or nearly flat surface of respectively width w, with rounded corners of radius r (see figure 3.2), the useful width is calculated in the following way:

$$b_{eff} = w - 2r \tag{3.3}$$

In case of a flange running wheel, as shown in figure 3.2, the useful width is calculated using the following formula:

$$b_{eff} = w - r \tag{3.4}$$

The equivalent diameter is dependent on the contact method, as shown in figure 3.3. The three contact methods are:

- Wheel-on-Wheel: $D_{eq} = \frac{D_1 D_2}{D_1 + D_2}$
- Wheel-on-Surface: $D_{eq} = D_1$
- Wheel-in-Wheel: $D_{eq} = \frac{D_1 D_2}{|D_1 - D_2|}$

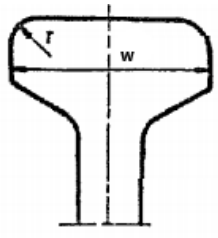

Figure 3.1: Rail dimensions explained [37]

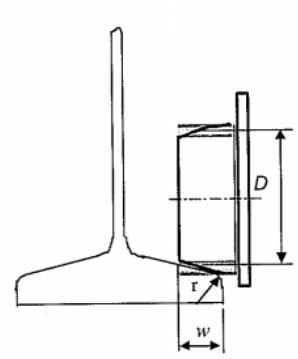

Figure 3.2: Flange running wheel dimensions [37]

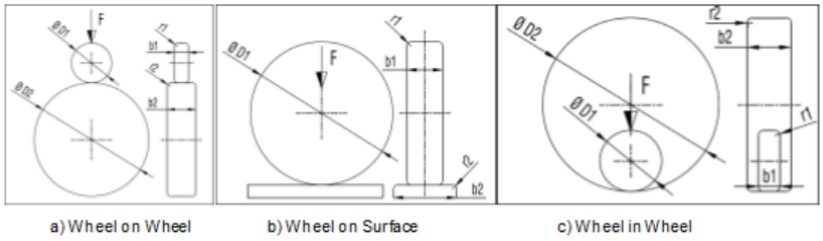

Figure 3.3: The three different contact methods [3]

For the standards used by Huisman, the equivalent diameter contact method is always wheel-on-surface.

The limiting pressure P_L depends on the ultimate strength of the wheel material σ_u as explained by ISO 16881 [37]. This is shown in figure 3.1, together with the minimum ultimate strength the wheel requires for this limiting pressure.

Ultimate strength of metal used for rail wheel, N/mm^2	Limiting pressure P_L	Minimum ultimate strength rail, N/mm^2
>500	5	350
>600	5.6	350
>700	6.5	510
>800	7.2	510
>900	7.8	600
>1000	8.5	700

Table 3.1: Limiting pressure based on wheel material ultimate strength

3.1.2. Fatigue Load Cases

The FEM/ISO method does not define a maximum allowed force directly, but rather an allowed average load:

$$F_{mean} = \frac{F_{minA,B} + 2F_{maxA,B}}{3} \leq P_L b_{eff} D_{eq} c_1 c_2 \tag{3.5}$$

The difference between this equation and the equation for the allowed static force is that the factor 1.9 is replaced with two new factors: c_1 and c_2.

c_1 is dependent on the rotation speed of the wheel, and is obtained using table **??** [37]:

Wheel rotation speed r/min	c_1	Wheel rotation speed r/min	c_1	Wheel rotation speed r/min	c_1
200	0,66	50	0,94	16	1,09
160	0,72	45	0,96	14	1,10
125	0,77	40	0,97	12,5	1,11
112	0,79	35,5	0,99	11,2	1,12
100	0,82	31,5	1	10	1,13
90	0,84	28	1,02	8	1,14
80	0,87	25	1,03	6,3	1,15
71	0,89	22,4	1,04	5	1,16
63	0,91	20	1,06		
56	0,92	18	1,07		

Table 3.2: values for c_1 [37]

c_2 depends on the mechanism class, which itself is dependent on two factors: the utilization class and the Spectrum class [37].

Spectrum Class	Utilization Class									
	T0	T1	T2	T3	T4	T5	T6	T7	T8	T9
L1	1.25	1.25	1.25	1.25	1.12	1.12	1	0.9	0.8	0.8
L2	1.25	1.25	1.25	1.12	1.12	1	0.9	0.8	0.8	0.8
L3	1.25	1.25	1.12	1.12	1	0.9	0.8	0.8	0.8	0.8
L4	1.25	1.12	1.12	1	0.9	0.8	0.8	0.8	0.8	0.8

Table 3.3: values of c_2 [3]

The utilisation class is dependent on the total duration of use in hours:

Utilization class	total duration of use T(h)		
T0	0	≤T≤	200
T1	200	<T≤	400
T2	400	<T≤	800
T3	800	<T≤	1600
T4	1600	<T≤	3200
T5	3200	<T≤	6300
T6	6300	<T≤	12,500
T7	12,500	<T≤	25,000
T8	25,000	<T≤	50,000
T9	50,000	<T≤	∞

Table 3.4: Utilisation class[3]

The Spectrum class is dependent on the Force spectrum factor k_c:

Spectrum class	Spectrum factor k_c(-)		
L1	0	$< k_c \leq$	0.125
L2	0.125	$< k_c \leq$	0.250
L3	0.250	$< k_c \leq$	0.500
L4	0.500	$< k_c \leq$	1.000

Table 3.5: Spectrum class[3]

The Force spectrum factor is given by:

$$k_c = \frac{1}{k_{fs}} \sum_{i=1}^{k_{fs}} \left(\frac{F_i}{F_{max}} \right)^m \tag{3.6}$$

Where

- i is the current rolling contact with force F_i
- k_{fs} is the total amount of rolling contacts
- F_i is the force during rolling contact i
- F_{max} is the maximum occurring force from the load cases
- m is the exponent for wheel/rail contacts: $m = 10/3$

The force spectrum factor reverses an S-N curve by implementing factor m which represents the slope in an S-N curve, while also implementing miner's rule by calculating how much of the lifetime is used up per load case.

3.1.3. Hardening Depth

The FEM/ISO method uses a very simple method for determining the hardening depth, merely dependent on the equivalent diameter D_{eq}:

$$\delta = 0.01 D_{eq} \tag{3.7}$$

3.2. EN 13001-3-3 [3] [35]

The EN 13001 is an European standard which focuses on the design of cranes. Where En 13001-1 focuses on the general principles and requirements, En 13001-2 focuses on the specific load actions and combinations that cal occur. These will be used in EN 13001-3 to design the specific parts of the crane, where EN 13001-3-3 focuses on wheel/rail contacts. The EN 13001-3-3 is the preferred method by Huisman. An advantage is a more detailed description of the problem compared to the FEM/ISO method. It does, however, have a limited range at which it can be applied. It can only be used if:

- $r_k > 5 * min(b_r; b_w)$, in which case the contact is considered a point contact
- $r_k > 200 * min(b_r; b_w)$, in which case the contact is considered a line contact

Where r_k is the crown radius of the rail or wheel, and b_r and b_w are the effective contact widths of the rail and wheel, as shown in figure 3.4. If the radius does not fulfil this requirement, the Horowitz method for ball on surface contact can be used. Since most of the Huisman wheels will fall under a point contact, only this type of contact is covered for EN 13001-3-3.

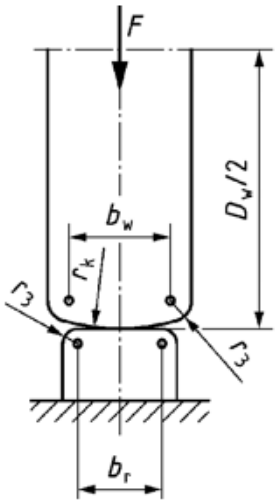

Figure 3.4: Wheel and rail dimensions including crown radius [35]

3.2.1. Static Load Cases

For EN 13001-3-3, the allowed static load is given by the following equation:

$$F_{Static} = \frac{A_s^2 \pi D_{eq} b_{eff} (1-\upsilon^2)}{E_m \gamma_{cf}} f_1 f_2 \tag{3.8}$$

Where:

- υ is the Poisson ratio, which is 0.3 for steel
- A_s Is the Static Hardening factor
- f_1 is the edge pressure safety factor
- E_m is the Equivalent Elastic modulus: $E_m = \frac{2E_1E_2}{E_1+E_2}$
- f_2 is the non-uniform pressure distribution safety factor
- γ_{cf} is the general resistance coefficient: $\gamma_{cf} = 1.1$
- D_{eff} and b_{eff} are as explained in chapter 3.1.1

The static hardening factor is dependent on the material hardness. If the Brinell hardness HB is at least 0.6 times the yield stress σ_y, the material is considered hardened.
-For non-hardened materials: $A_s = 7 * HB$ where HB is the Brinell hardness of the material.
-For hardened materials: $A_s = 4.2 * \sigma_y$

The edge pressure safety factor f_1 is set to 1.0 for point contact. For line contact, the factor is dependent on the width of the projecting non-contact area w and the radius of the edge of the non-projecting part (see figure 3.6)

The non-uniform pressure distribution f_2 is 1.0 for point contact. For line contact, it is dependent on the aligning of the wheel and rail, and the tolerance class of the crane. The tolerance class is dependent on the total travelling distance in km as shown in figure 3.7. The resulting values for f_2 are shown in figure 3.12.

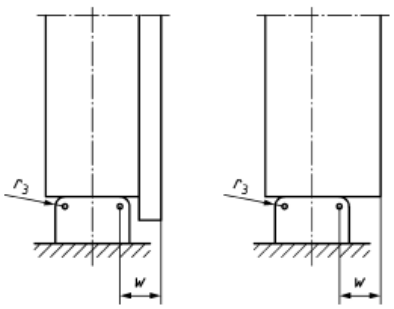

Ratio r_3/w	Factor f_1
$r_3/w \leq 0{,}1$	0,85
$0{,}1 < r_3/w < 0{,}8$	$[0{,}58 + 0{,}15\,(r_3/w)]/\,0{,}7$
$r_3/w \geq 0{,}8$	1,0
where w is the width of the projecting non-contact area and r_3 is the radius of the edge of the non-projecting part (wheel or rail).	

Table 3.6: Edge pressure determination [35]

Tolerance class	Limits of travelling and traversing distance km
1	$50\,000 \leq L$
2	$10\,000 \leq L < 50\,000$
3	$L < 10\,000$, for stationary erected tracks
4	Temporarily erected tracks for building and erection purposes

Table 3.7: Tolerance classes dependent of total travelling distance[1]

	Tolerance class of ISO 12488-1			
	1	2	3	4
Wheels with self-aligning mounting	1,0	1,0	0,95	0,9
Non-aligning wheel mounting, rail mounted on elastic support	0,95	0,9	0,85	0,8
Non-aligning wheel mounting, rail mounted on rigid support	0,9	0,85	0,8	0,7

Table 3.8: Values of f_2 [35]

3.2.2. Fatigue Load Cases

The allowed fatigue force according to the EN 13001-3-3 standard is a given formula:

$$F_{fatigue} = \frac{f_u}{\gamma_{cf}\sqrt[m]{s_{c,i}}} f_f \tag{3.9}$$

Where:

- f_u is the reference contact force
- s_c is the contact force history parameter
- m is the wheel/rail contact exponent: $m = 10/3$
- f_f is the factor of further influences
- γ_{cf} is the general resistance coefficient: $\gamma_{cf} = 1.1$

The reference force f_u is calculated using:

$$f_u = \frac{A_f^2 \pi D_{eq} b_{eff} (1-\nu^2)}{E_m} \tag{3.10}$$

Where A_f is the hardening factor for fatigue, which depends on the hardness of the material. Just like the static hardening factor, a material is considered hardened if the Brinell hardness is at least 0.6 times the yield stress σ_y.
-$A_f = 1.8\sigma_y$ if the material is hardened
-$A_f = 3HB$ if the material is not hardened

The contact force history parameter is given by $S_c = k_c \times \nu_c$, where:
-Reference rolling contacts $\nu_c = \frac{n_{tot}}{n_D}$ with n_{tot} the total amount of revolutions / roll overs and $n_D = 6.4 * 10^6$
-Force spectrum factor k_c, as explained in equation 3.6

The factor of further influences f_f is given by:

$$f_f = f_{f1} f_{f3} f_{f4} \tag{3.11}$$

Where:

- f_{f1} is the edge pressure factor, which is equal to f_1 from the static load cases, see equation 3.8
- f_{f3} is the skewing factor, which accounts for increased wear due to the skew angle α. For $\alpha \leq 0.005$ rad, $f_{f3} = 1$. For $\alpha > 0.005$ rad:
$$f_{f3} = \sqrt[3]{\frac{0.005}{\alpha}} \tag{3.12}$$
- f_{f4} is a factor which takes mechanical abrasion effects into account in unclean environments.
-$f_{f4} = 0.95$ for driven wheels in environment with abrasive particles
-$f_{f4} = 1.0$ for non-driven wheels or wheels in an environment without abrasive particles.

Rewriting this set of equations results in a rather complicated equation for the allowed rotations for a certain force F_i:

$$N_f = \left(\frac{A_f^2 \pi D_{eq} b_{eff} (1-\nu^2)}{E_m \gamma_{cf} F_i} f_f \right)^m \frac{i_D}{k_{c,i}} \tag{3.13}$$

Where i_D is the number of rolling contacts at reference point: $i_D = 6.4 * 10^6 (-)$, which is defined identically to previously mentioned n_D. Since this value is calculated for each load case individually, $k_{ci} = 1$. When filling in all other known values reduces the equation to a more simple form:

$$N_f \approx 1.54 * 10^8 \left(\frac{A_f^2 D_{eq} b_{eff}}{E_m F_i} f_f \right)^{\frac{10}{3}} \tag{3.14}$$

3.2.3. Hardening Depth

According to EN 13001-3-3, the required hardness is determined as twice the depth of the highest shear stress value. This results in the following set of equations:

For line contact:

$$\delta = 2 * 0.5 * \sqrt{\frac{F_{max} \pi D_{eq} (1-\nu)^2}{b_{eff} E_m}} \tag{3.15}$$

For steel ($\nu = 0.3$), this reduces to:

$$\delta = 1.69 \sqrt{\frac{F_{max} D_{eq}}{b_{eff} E_m}} \tag{3.16}$$

For point contact:

$$2 * 0.68 * \sqrt[3]{\frac{F_{max}}{E_m} * \frac{1-\nu^2}{\frac{2}{D_w} + \frac{1}{r_k}}} \tag{3.17}$$

Where:

- D_w is the wheel diameter
- r_k is the wheel curvature radius of the wheel
- F_{max} is the maximum occurring force from the load cases

3.3. Horowitz [3] [38]

Prof. ir. A. Horowitz designed a method which describes the geometry for a cylindrical roller [38]. Is uses the Hertzian stresses within the contact. Horowitz used to be the calculation method used by Huisman. However it is not be used anymore since he EN13001 method is now preferred.

3.3.1. Static Load Cases

For Horowitz, the allowed static force is not defined as the maximum static load case that the wheel or rail can withstand, but the allowed static force is assumed to be the fatigue force for a very low amount of rotations. Therefore, the equivalent static rotations N_{static} need to be found. Since for FEM/ISO the static rotations are zero, the EN 13001-3-3 rotations are used.

$$N_{static} = \left(0.18 \frac{f_{f3} f_{f4}}{f_2}\right)^{\frac{10}{3}} i_D \tag{3.18}$$

Where:

- f_{f3} is the skewing factor as explained in equation 3.12
- f_{f4} is the mechanical drive factor, which is explained for equation 3.11
- f_2 is the factor for non-uniform pressure distribution, as explained in chapter 3.2.1.

Furthermore, the Hertz-stress method is used which calculates the stress under rolling contact:

$$\sigma_{H,i} = 0.591 \sqrt{\frac{F_i * E_m}{b_{eff} * D_{eq}}} \tag{3.19}$$

Where:

- F_i is the force that occurs in the load case
- b_{eff} and D_{eq} are as explained in chapter 3.1.1

Horowitz includes the influence of a new value called the Stribeck value. This way, the allowed Hertz stress for a load case i is:

$$\sigma_{H,i} \leq 10 k_{h,i} HB \tag{3.20}$$

Where:

- HB is again the Brinell Hardness
- $k_{h,i}$ is the Stribeck value, which is given by:

$$k_{h,i} = max((0.812 - 0.07 log(n_i)), 0.27) \tag{3.21}$$

Here, n_i is once again the number of rotations / over rolls for the current load case

This all together will result in the allowed static force:

$$F_{static} = \frac{b_{eff} D_{eq}}{E_m} \left(\frac{(0.812 - 0.07 log(N_{static})) * 10 HB}{0.591}\right)^2 \tag{3.22}$$

3.3.2. Fatigue Load Cases

The number of allowed rotations is calculated by rewriting the equation for static load, which results in the following equation for the allowed number of rotations until failure N_i dependent on the load F_i:

$$N_i = 10^{\left(-0.844\sqrt{\frac{F_i E_m}{b_{eff} D_{eq} HB^2}}+11.6\right)} \tag{3.23}$$

Implementing the equation for the Hertz stress as described in equation 3.19 results in the following simplified equation for allowed number of cycles until failure:

$$N_i = 10^{\left(\frac{-\sigma_H}{0.7*HB}+11.6\right)} \tag{3.24}$$

3.3.3. Hardening depth

According to the Horowitz method, the required hardening depth for line contact is given by:
-Line contact: $\delta = 0.78b$
-Point contact: $\delta = 0.48b$

Where:

$$b = 4\frac{\sigma_h D_{eq} * (1-\upsilon^2)}{E_m} \tag{3.25}$$

When substituting the equations for Hertz stress $\sigma_{H,i}$ as shown in equation 3.19, and the Poisson ratio $\upsilon = 0.3$ for steel, the hardening depth is calculated as:

For line contact:

$$\delta = 1.68\sqrt{\frac{F_{max} D_{eq}}{b_{eff} E_m}} \tag{3.26}$$

For point contact:

$$\delta = 1.03\sqrt{\frac{F_{max} D_{eq}}{b_{eff} E_m}} \tag{3.27}$$

3.4. Differences

The three main calculation methods used by Huisman have been discussed, and have shown to have many differences. It is therefore important to take a closer look at the differences and why they are different.

3.4.1. Static Load Cases

All three different methods show that the allowed static load scales linearly with the elastic modulus E, the effective width b_{eff} and the equivalent diameter D_{eq}. Besides these two parameters, the calculation of the allowed static load is dependent on different parameters for all three methods.

- The FEM/ISO method shows in equation 3.2 that the allowable static load also scales linear with the limiting pressure P_L, which in itself is only dependent on the ultimate strength of the material.

- The EN 13001-3-3 method shows a lot more input parameters shown in equation 3.8, of which the Static hardening factor A_s and the Equivalent elastic modulus E_m are dependent on material properties, while the edge pressure safety factor f_1 is dependent on the contact type and geometry of the wheel/rail contact, and the non-uniform pressure distribution f_2 which is dependent on the total travel distance and the wheel alignment.

- The Horowitz method shown in equation 3.22 also calculates the allowed static load depending on material properties, which are the equivalent elastic modulus E_m and the Brinell hardness HB. However, the biggest difference is that the Horowitz method also uses the equivalent static rotations N_{static}, which in itself is dependent on the skewing factor f_{f3}, the mechanical drive factor f_{f4} and and the non-uniform pressure distribution f_2.

The main difference between these methods is that the FEM/ISO method merely takes the basic geometry of the wheel and rail, and the ultimate strength into account, while the EN 13001-3-3 and Horowitz methods also take the equivalent elastic modulus and hardness properties into account. Additionally, these methods also take into account the more practical data, such as the contact type, travel distance and wheel alignment. The Horowitz method even takes skewing and mechanical abrasion effects into account, which makes it the most detailed way of calculating the allowed static load.

3.4.2. Fatigue Load Cases

Just like for the static load cases, the allowed fatigue load is for all three methods linearly dependent on the effective width b_{eff} and the equivalent diameter D_{eq}. Furthermore, all other influences are different per method.

- The FEM/ISO method shows again the linear dependence on the limiting pressure P_L, and therefore the ultimate strength of the material. In addition, it is now also dependent on factors c_1 and c_2, which include the travel speed in rpm, the total duration of use and the force spectrum factor k_c. These values are all taken from tables, and are not calculated linearly. Continuous formula can be created from the tables in order to state allowed load as a function of these parameters. However, since the parameters are directly from standards, this will not be implemented.
- The EN 13001-3-3 also calculated the allowed fatigue load similar to the allowed static load with the addition of the contact force history parameter S_c, which is dependent on the reference rolling contacts v_c and the force spectrum factor k_c, and the factor of further influences f_f, which adds the edge pressure factor f_1, skewing effects f_{f3} and mechanical abrasion effects f_{f4}.
- Horowitz uses the Stribeck value and the Brinell hardness to calculate the allowed Hertz stress. This results in an equation for the amount of rotations until failure N_i, which is derived from the same equation as the equation for allowed static force 3.22, which used the equivalent static rotations instead.

It becomes clear from all three methods that the allowed fatigue load is calculated similarly to the allowed static load with additional factors that include effects a like total distance traveled, force spectrum factor and more. Where the FEM/ISO method takes these factors from classification tables, the EN-13001-3-3 method includes them in the allowed fatigue load equation which creates a continuous formula. Since the Horowitz method already used the amount of rotations in the allowed static load as the equivalent static rotations N_{static}, this is transferred in the allowable fatigue load with the rotations now as the maximum amount of rotations until failure N_f.

3.4.3. Hardening depth

It is clear to see that the FEM/ISO method is a very much simplified method of calculating the hardening depth, since it is only dependent on the wheel diameter. The other methods go in much more detail, using material properties and the load cases, which could potentially allow for a lower hardening depth.

The Horowitz and the EN 13001-3-3 method, however, have more input variables and have many similarities. Especially for line contacts, the equations are almost identical, as shown in equations 3.16 and 3.26. The only difference is the multiplication factor (1.68 for Horowitz, 1.69 for EN 13001-3-3). However, this is assuming a Poisson ratio v of 0.3. Since the depth is dependent on $(1-v^2)$ for Horowitz, but $\sqrt{(1-v^2)}$ for EN 13001-3-3, the multiplication factors of both methods can differ a lot more when other materials are considered. However, since all wheels designed by Huisman are steel wheels, the methods can be considered almost identical.

For point contact, the calculations done by Horowitz and the EN 13001-3-3 method are very different. Where Horowitz just uses a different multiplication factor for line and point contact, as seen in chapter 3.3.3, the EN 13001-3-3 method defines the required depth is twice the depth of highest shear stress, which for point contact results in a very different equation then for line contact, as seen in chapter 3.2.3. This method is also dependent on the radius of the wheel and the crown radius. Since it is defined as twice the depth of maximum shear stress, it makes sure that the wheel is hardened in the area of highest shear stresses.

4

Analytical Model Results

This chapter will show the differences between the different methods based on two different real life example wheels used by Huisman equipment. This will be done according to an analytical model based on the theories and equations stated in chapter 2 and 3, modeled using Microsoft Excel Excel Visual Basic for Applications (VBA). It aims on answering the final sub-question stated in the introduction:

How do the results of the fracture mechanics calculations compare to the calculations using methods according to standards, and how to determine which method is most realistic?

Firstly, the real life example wheels that are used are shown, and their parameters and dimensions are explained. Then, the allowed static load according to the EN 13001 and Horowitz methods will be implemented. Afterwards, the results for all four different methods will be compared. Finally, since many of the fracture mechanics parameters are estimated in literature, the effects of these parameters is analyzed by changing these. This will show how much effect certain parameters have on the lifetime of the wheels.

4.1. Input Parameters Example Wheels

The calculations will be done for two real life example wheels which are currently in use in certain Huisman equipment. The first wheel is a 1600mm diameter wheel on a raceway, and the second wheel is a 300mm diameter wheel used in bogies. Illustrations of the wheels are shown in appendix B to give a clear perspective of how the wheels look in real life. The purpose for both wheels will be explained, and their input parameters will be defined. Afterwards, the fracture mechanics input parameters will be defined.

4.1.1. 1600mm Wheel

This 1600mm wheel is used in a motion-compensated gripper system, which is used for placing monopiles. It's purpose in the system is to allow for motion in the longitudinal direction. The parameters needed are shown in the design report and shown in figure 4.1.

DEME Gripper X Skid front Z		A19-47000		
	Symbol	Wheel	Rail	Unit
Diameter	d	1600		mm
Width	b	450	460	mm
Edge radius	r	5	5	mm
Wheel curvature	rk	40000		mm
Material		30CrNiMo8	HB400	
Youngs modulus	E	210000	210000	Mpa
Yield sress		648	1000	MPa
Ultimate stress		818	1250	MPa
Brinell-Hardness		333	350	-
Hardened BH		480		-
Hardening limit		5		mm
factor further infl	ff	1		-

Table 4.1: Known input parameters for the 1600mm wheel

In order to calculate the allowed load according to the methods described by the standards, the input parameters which are not stated in the design report are defined.

FEM/ISO

- Flange running wheel: The wheel is not a flange running wheel. This can be seen in figure B.1in appendix B.
- Wheel rotation speed: Although not directly stated in the design report, it is assumed that the wheel travels $600mm$ in 6 seconds, which results in a rotation speed of 1.19 rpm.
- Spectrum factor $k_c = 1.0$.

En 13001 & Horowitz

Factors of further influence $f_f = 1$ is defined in the design report. Therefore, the following assumptions can be made:

- Wheel alignment: Assumed self-aligning mounting chosen so that $f_2 = 1$ in order to comply with the fact that factors of further influence $f_f = 1$.
- Abrasive particles present?: No, Resulting in $f_f = 1$.
- Total skew angle: Assumed to be $\alpha \leq 0.005$ rad in order to comply with $f_f = 1$.

4.1.2. 300mm Wheel

These 300mm Wheels are used for the top drive bogies for a Dual Multi Purpose Tower (DMPT), which is used for drilling. Again, the parameters are given in the wheel design report, and are shown in figure 4.2

Bogies top drive 680mt DMPT		A18-42610		
	Symbol	Wheel	Rail	Unit
Diameter	d	300		mm
Width	b	119	60	mm
Edge radius	r	29.5	0	mm
Wheel curvature	rk	1500		mm
Material		30CrNiMo8	HB400	
Youngs modulus	E	210000	210000	Mpa
Yield sress		500	650	MPa
Ultimate stress		800	1250	MPa
Brinell-Hardness		333	240	-
Hardened BH		530		-
Hardening limit		4		mm
Factor further infl	ff	1		-
Spectrum fac	kc	0.7		-
Tolerance class		2		-
vc	vc	6.5		-

Table 4.2: Known input parameters for the 300mm wheel

Again, the input parameters which are not stated in the design report are defined.

FEM/ISO

- Flange running wheel: The wheel is not a flange running wheel. This can be seen in the technical drawing shown in figure B.2 in appendix B.
- Wheel rotation speed: Although not directly stated in the design report, it is estimated that the wheel travels 2 meters in 6 seconds, which results in a rotation speed of 21.22 rpm.

En 13001 & Horowitz

Just as for the 1600 wheel, factors of further influence $f_f = 1$ is defined in the design report, resulting in identical assumptions.

4.1.3. Fracture Mechanics Input Parameters

For both wheels, the same fracture mechanics input parameters will be used, as shown in table 4.3.

Geometry factor	Y	1	-
Friction coefficient	k	0.78	-
Initital crack size	a_0	0.1	mm
Step size	ΔN	1000	cycles
Minimum stress	σ_min	0	Mpa
Paris law exponent	n	3	-
Intercept constant	C_0	5.21E-13	-
Walker constant	γ	0	-
Threshold K	ΔK_th	50	MPa
Fracture toughness	K_c	100	MPa
NASGRO coefficient p	p	0	-
NASGRO coefficient q	q	0	-
Newman crack closure	f	0	-

Table 4.3: Fracture mechanics input parameters used

4.2. Allowed Static Load

Besides fatigue load cases, the EN13001 and Horowitz methods also calculate an allowable static load. This limit is independent of the amount of cycles. When comparing the allowable static load against the allowable fatigue load for both the 1600mm and 300mm wheel using the EN13001 method, the resulting figures show an interesting result:

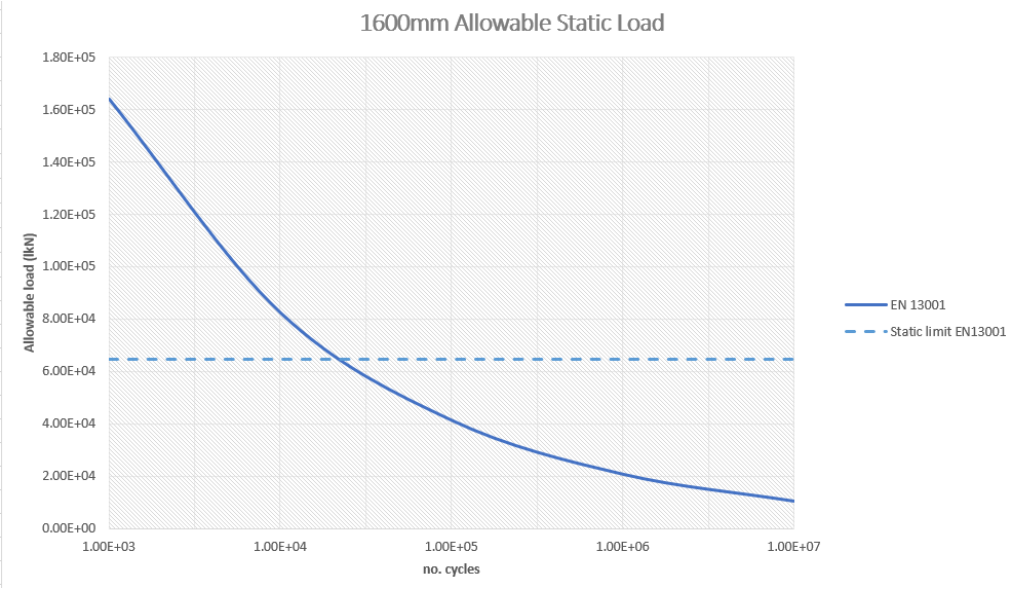

Figure 4.1: 1600mm wheel comparison between the fatigue load and static load for EN13001

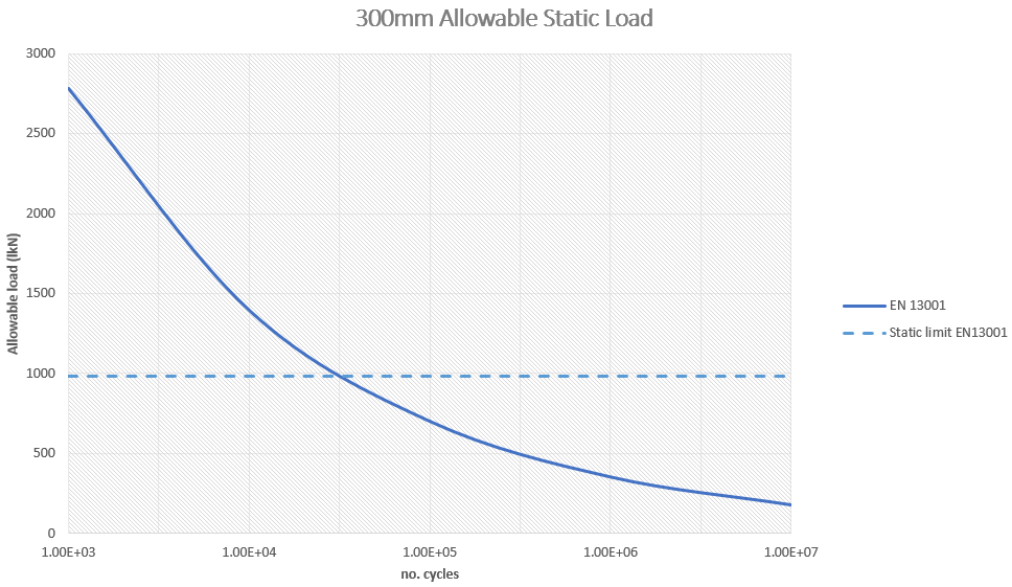

Figure 4.2: 300mm wheel comparison between the fatigue load and static load for EN13001

The results show that the allowable static load is lower then the allowable fatigue load for low numbers of cycles. This indicates that the allowed load calculations for a low cycle number must be dependent on the minimum of the static and fatigue load calculations for this method. The Horowitz method shows comparable results, as shown in figure 4.3 and figure 4.4. This indicates that the allowable load calculations for both the EN13001 and Horowitz method are dependent on both fatigue and static load calculations.

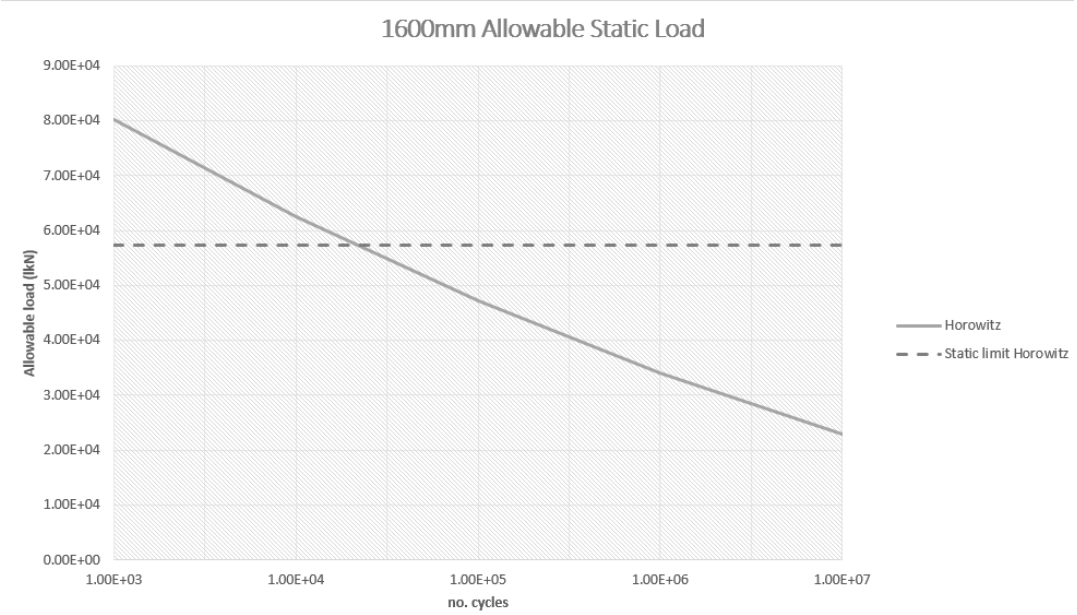

Figure 4.3: 1600mm wheel comparison between the fatigue load and static load for Horowitz

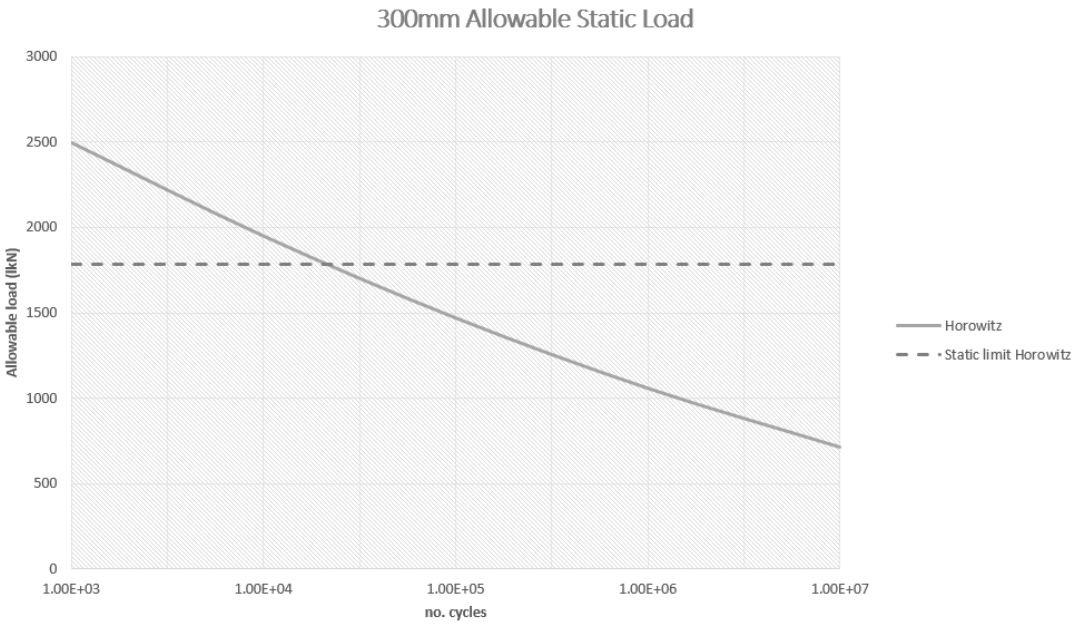

Figure 4.4: 300mm wheel comparison between the fatigue load and static load for Horowitz

4.3. Comparison Between the Methods

The input parameters shown in the previous section will be used to calculate and visualize the relation between the allowed load and the lifetime of the wheels according to all four methods. The results for both wheels will be discussed after the results are shown for both wheels first.

4.3.1. 1600mm Wheel

For the 1600mm wheel, the different methods are compared in the graph and table shown below.

Figure 4.5: Results for all methods plotted for the 1600 mm wheel

Cycles	Load (kN)			
-	FEM/ISO	EN13001	Horowitz	Fracture mechanics
1000	7.40E+03	1.64E+05	8.01E+04	3.83E+04
10000	7.40E+03	8.24E+04	6.26E+04	3.59E+04
100000	6.60E+03	4.13E+04	4.72E+04	2.32E+04
1000000	4.70E+03	2.07E+04	3.40E+04	6.60E+03
10000000	4.70E+03	1.04E+04	2.29E+04	1.04E+03

Table 4.4: Resulting values of all methods for the 1600 mm wheel

The results show that with these assumed input parameters, the allowed load according to fracture mechanics is lower then for the EN13001 and Horowitz methods. Also, the fracture mechanics method follows a different trend then the EN13001 and Horowitz method, as it does not have an increased slope at lower number of cycles. Implementing the allowed static load results in comparable trends. If certain fracture mechanics input parameters are estimated differently, the results can change. This will be analyzed in section 4.5.

4.3.2. 300mm Wheel

For the 30000mm wheel, the different methods are compared in the graph and table shown below.

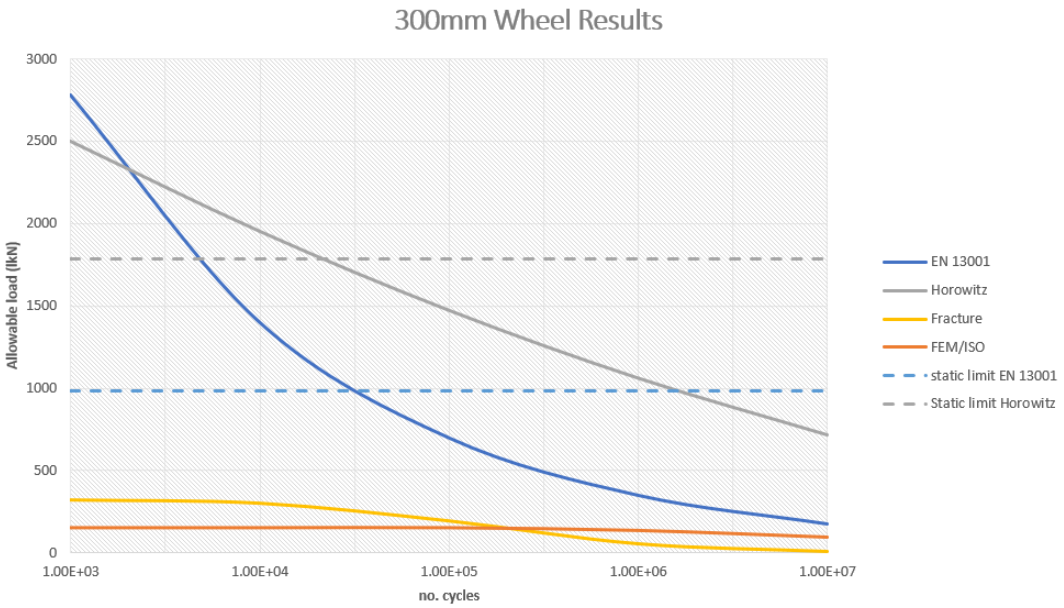

Figure 4.6: Results for all methods plotted for the 300 mm wheel

Cycles	Load (kN)			
-	FEM/ISO	EN 13001	Horowitz	Fracture mechanics
1000	1.54E+02	2.78E+03	2.50E+03	3.24E+02
10000	1.54E+02	1.40E+03	1.95E+03	3.04E+02
100000	1.54E+02	6.99E+02	1.47E+03	1.96E+02
1000000	1.38E+02	3.50E+02	1.06E+03	5.60E+01
10000000	9.83E+01	1.76E+02	7.14E+02	9.00E+00

Table 4.5: Resulting values of all methods for the 300 mm wheel

The results for the 300mm wheel assuming said input parameters show comparable aspects as the 1600mm wheel, such as the fact that the values for the fracture mechanics method are lower then the EN13001 and Horowitz methods, and the trend is different. However, with the 300mm wheel, the difference between the fracture mechanics method and the EN13001 and Horowitz methods is much larger then for the larger 1600mm wheel. This is very dependent on the assumed fracture mechanics parameters. If these parameters are assumed differently, the values of the fracture mechanics result may be different.

4.4. Analyzing the Results

For both the 1600 and the 300mm wheel, the FEM/ISO method shows a much lower allowed load than the other methods. The tables for both wheels also show that many data points of the FEM/ISO methods are identical. This is due to the fact that the FEM/ISO method is not a continuous relation, but a relation in discrete steps. It can be assumed that the FEM/ISO method is not suitable for these applications, since the allowed load is not varying as much compared to the other methods. To verify this assumption, however, experimental data is needed.

The EN 13001 and Horowitz methods are much more alike. They both show an increasing slope at a lower number of cycles, which is visible in both examples. However, the change of this slope is larger for the EN 13001 method than the Hertz stress based Horowitz method. It is also interesting to see the relations of both methods cross each other, but the number of cycles where this occurs is different for each example wheel. This is due to the differences between both methods in using certain input parameters to calculate lifetime.

The difference in slope might be caused by the calculation on the Hertz stress. The Horowitz method calculates the Hertz stress as described in equation 3.19, where it is dependent on the force F, the elastic modulus E and the geometry of the wheel/rail contact b_{eff} and D_{eq}. However, it is not dependent on the wheel curvature radius r_k, which would suggest that it is calculating the Hertz contact pressure for cylindrical contact. According to the criterion stated by the EN 13001 standard shown in section 3.2, the contact is considered a point/elliptical contact. This is confirmed by comparing the Hertz stress values of both the cylindrical and elliptical contact theories to the Hertz stress value as described by the Horowitz method and an FEA model of the contact using the 1600 mm wheel input parameters and an input load of 500 kN. The wheel/rail model is illustrated in figure 4.7.

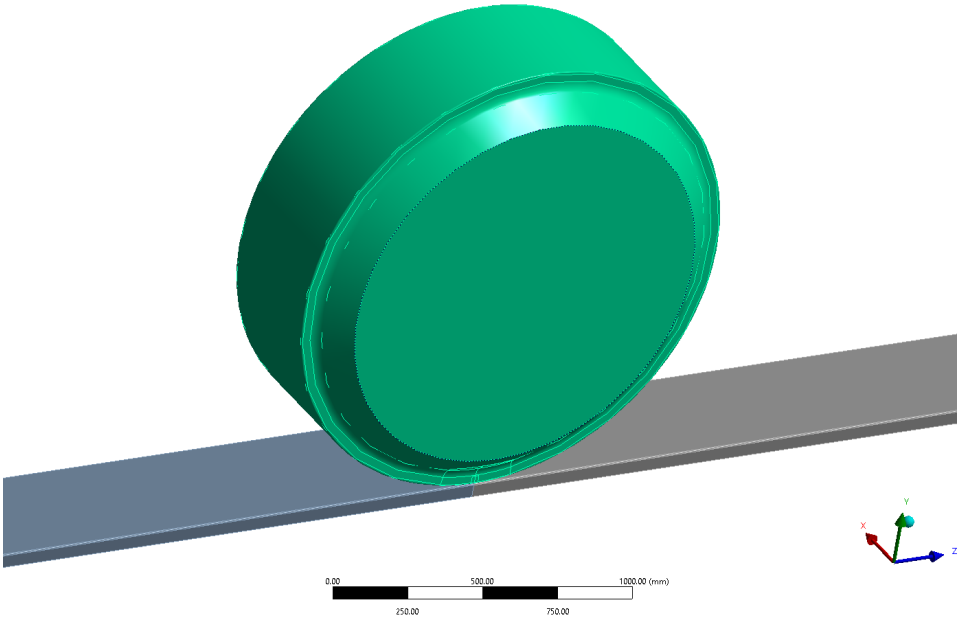

Figure 4.7: Mesh of the model illustrated (wheel not visible)

This FEA model is created in ANSYS, and uses three different mesh sizes:

- 1 mm mesh size close to contact area, where stresses vary a lot over small distances, and detailed analysis is required.
- 5 mm mesh size transition area around the contact area, where stresses are low and not varying much.
- 200 mm mesh size (default) for the rest of the geometry, where stresses are nearly 0.

The mesh is illustrated in figure 4.8.

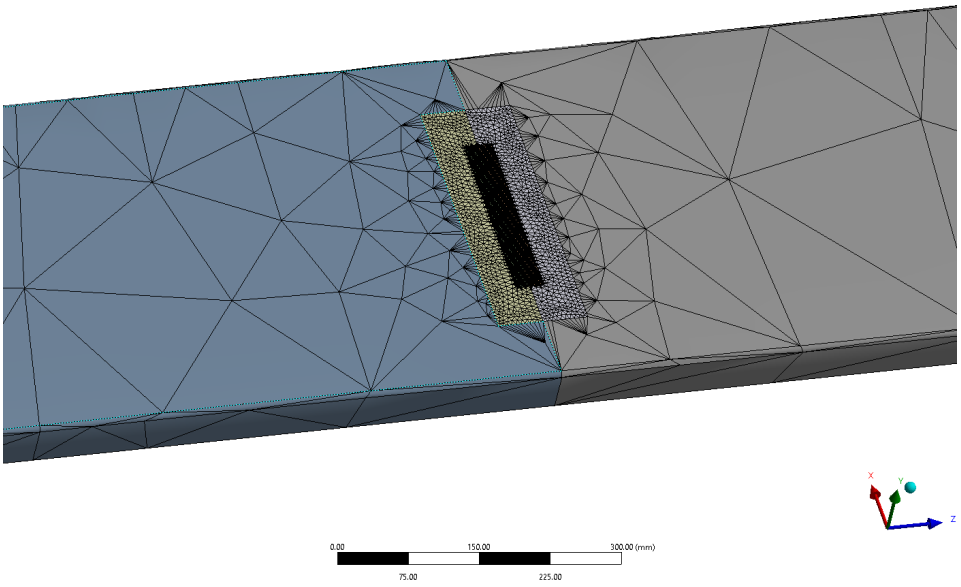

Figure 4.8: Mesh of the model illustrated (wheel not visible)

The resulting value for the Hertz stress is shown in table 4.6:

Horowitz Method	Cylindrical Hertz	Elliptical Hertz	FEA Model
228.4 Mpa	228.4 Mpa	470.8 Mpa	453 Mpa

Table 4.6: Comparison of the Hertz contact pressure as described by different methods

The results show that the FEA model value for maximum contact pressure is close to the value for elliptical Hertz contact pressure, which indicates that the Horowitz method does not calculate the Hertz stress correctly by assuming cylindrical contact. Analyzing the contact using an FEA model illustrates that the contact is indeed an elliptical contact, as shown in figure 4.9. This can be dependent on the load applied. This is a figure of the contact at the rail (Only the contact part is visible) where the pressures are visualized.

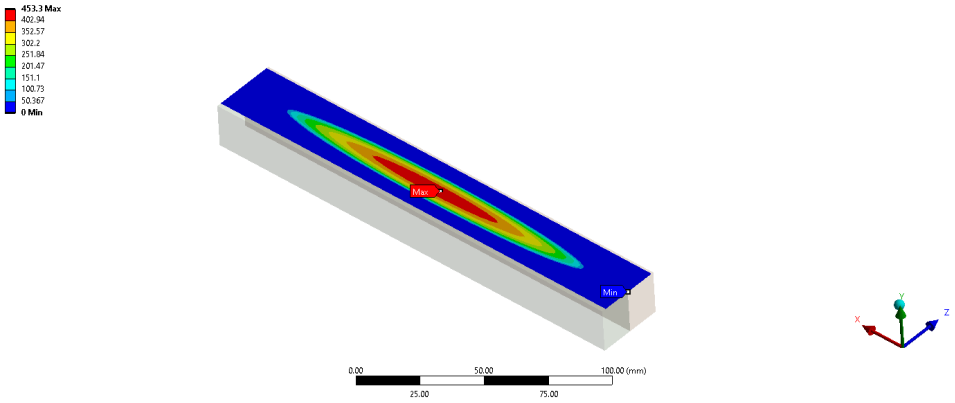

Figure 4.9: Results of the FEA model which show an elliptical contact

When using the Hertz stress for point/elliptical contact for the Horowitz method, the resulting allowable load changes. The changes are plotted, compared to the EN 13001 method for reference, in figure 4.10 . The updated Horowitz model shows a more comparable trend to the EN 13001 method then before.

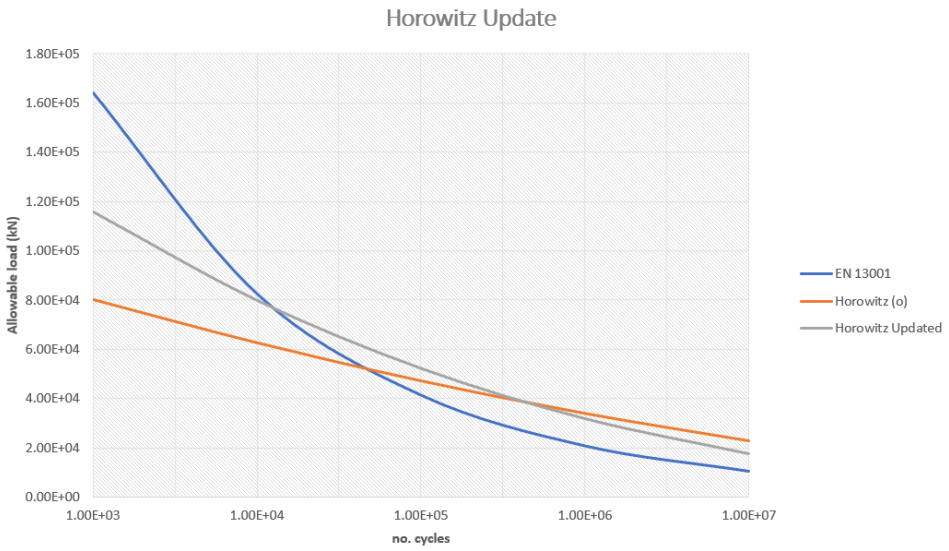

Figure 4.10: Comparison between the original Horowitz method (o), the updated Horowitz method, and the EN 13001 method

In order to give a clear comparison between the existing methods in this thesis and for consistency, the Horowitz method will not be updated, meaning, the original results for the Horowitz method will be used in this thesis.

As said before, fracture mechanics parameters have a large influence on the resulting values. This will be analyzed in the upcoming section.

4.5. Effects of Different Fracture Mechanics Parameters

Some parameters used in the fracture mechanics methods are not specified as a single value in literature, but different values and ranges are used in research and papers. This is due to differences in the steel used and the environment that the wheel operates in. The values used in this research may therefore not be the correct values in every different situation, and the resulting values and graphs can be very different. Three parameters which have the biggest uncertainty according to literature will be discussed in this section. The effects of changing these parameters will be illustrated, which gives a good insight in which parameters are most important to determine more precisely. This will be done using the 1600mm wheel example.

4.5.1. Effects of Initial Crack Size

The input parameters shown in previous sections show that the initial crack a_0 size used is 0.1 mm. The initial crack size of steel is usually between 0.05 and 3 mm, dependent on the type of steel used and how it is handled [39] [31]. Huisman assumes initial crack sizes of 0.1 mm for steels used in construction. Since the initial crack size can vary in practise, the effects of changing the initial crack size will be analyzed. The values used for initial crack size are:

- 0.06 mm
- 0.08 mm
- 0.1 mm (original value)
- 0.12 mm
- 0.14 mm

The resulting values are presented in a graph figure 4.11, with the addition of the EN 13001 results for reference. The values are also presented in table 4.7.

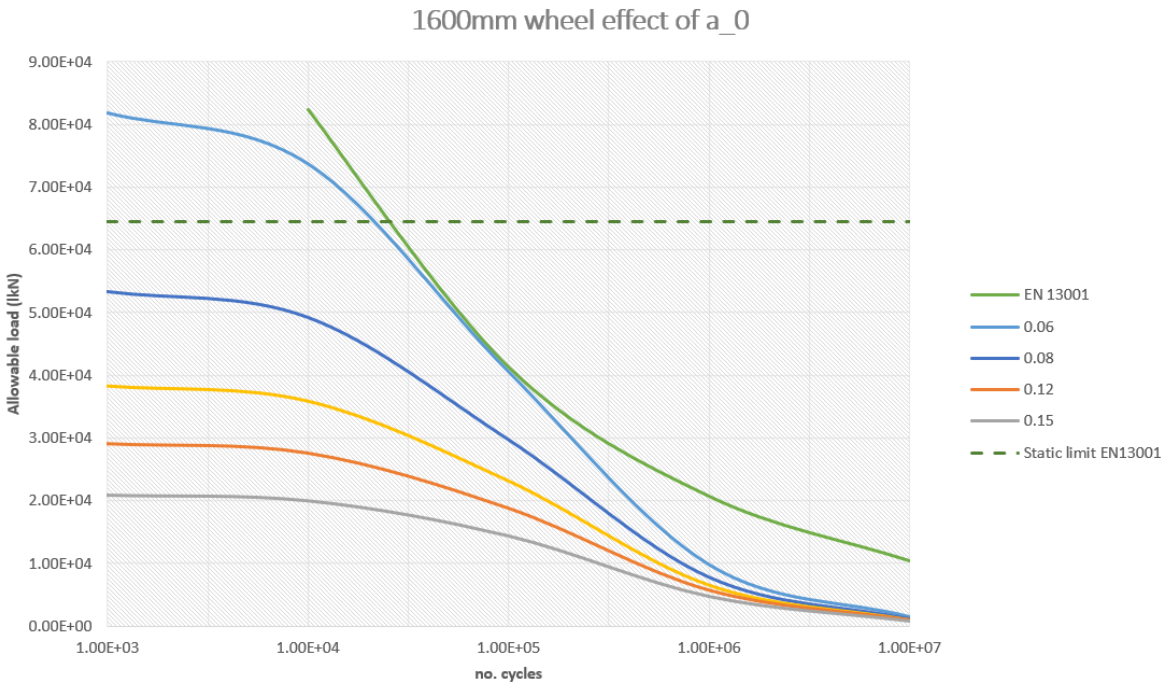

Figure 4.11: Results of varying the value of the initial crack size on the allowed load

Cycles	Load (kN)				
-	a_0 = 0.06	a_0 = 0.08	a_0 = 0.1	a_0 = 0.12	a_0 = 0.15
1000	8.19E+04	5.34E+04	3.83E+04	2.91E+04	2.09E+04
10000	7.38E+04	4.93E+04	3.59E+04	2.76E+04	2.00E+04
100000	4.06E+04	2.98E+04	2.32E+04	1.88E+04	1.44E+04
1000000	9.76E+03	7.85E+03	6.60E+03	5.70E+03	4.74E+03
10000000	1.42E+03	1.19E+03	1.04E+03	9.26E+02	8.00E+02

Table 4.7: Resulting values of changing the initial crack size a_0

The results show that the change in initial crack size creates larger changes in allowed load at lower number of cycles. Using a value of 0.06 instead of 0.1 more then doubles the allowed load for small numbers of cycles. Life expectancy for a wheel with a constant load will increase tremendously. However, the same trend remains when changing the initial crack size, and at large number of cycles. the allowed load remains nearly identical.

4.5.2. Effects of Fracture Toughness

The value of the fracture toughness K_c of structural steel is material specific and therefore varies widely. Values for steel range from 70 to 120 $MPa\sqrt{m}$. This is also dependent on the type of steel used. The values which are tested are:

- 80 MPa
- 95 MPa
- 100 MPa (original value)
- 110 MPa
- 120 MPa

The effects of changing the fracture toughness of the material are presented in the graph and table below. Again, the EN 13001 results are shown as reference.

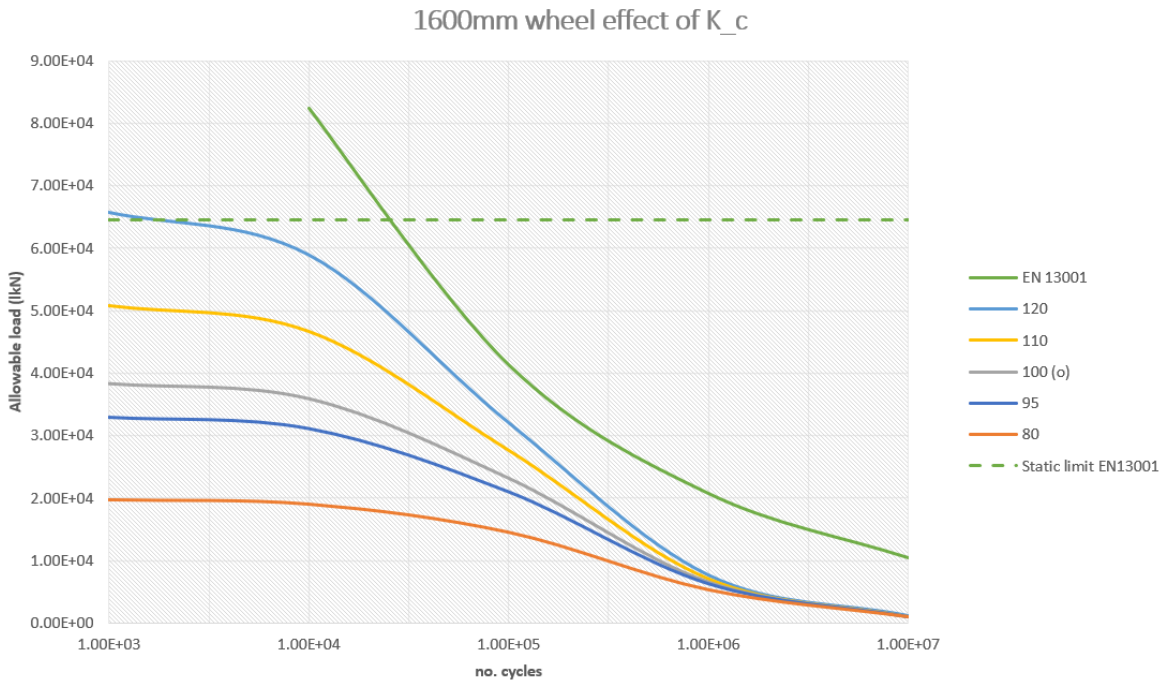

Figure 4.12: Results of varying the value of the fracture toughness on the allowed load

Cycles	Load (kN)				
-	$K_c = 80$	$K_c = 95$	$K_c = 100$	$K_c = 110$	$K_c = 120$
1000	1.97E+04	3.29E+04	3.83E+04	5.08E+04	6.58E+04
10000	1.90E+04	3.11E+04	3.59E+04	4.67E+04	5.90E+04
100000	1.45E+04	2.10E+04	2.32E+04	2.77E+04	3.21E+04
1000000	5.28E+03	6.30E+03	6.60E+03	7.14E+03	7.63E+03
10000000	9.50E+02	1.02E+03	1.04E+03	1.07E+03	1.11E+03

Table 4.8: Resulting values of changing the fracture toughness K_c

The results are comparable to the previously shown results of changing the initial crack size. Changes appear to be larger at lower numbers of cycles and low at high number of cycles, but the trend remains identical. The difference is that the changes due to the fracture toughness are small in comparison to the changes created by changing the initial crack size.

4.5.3. Effects of Intercept Constant

The intercept constant C_0 used in the Paris' equation has many different values according to literature. In this research, the value according to the BS 7910 [26] for steel in marine environment is used, which is $C_0 = 5.21E-13$. However, other literature, such as [27], show different values for C_0, which can range between 10^{-11} and 10^{-15}. Therefore, the following values of C_0 will be used:

- 5.21 E-11
- 5.21 E-12
- 5.21 E-13 (original value)
- 5.21 E-14
- 5.21 E-15

The results are shown in figure 4.13, which again includes the results for EN13001 as reference. Values are presented in figure 4.9.

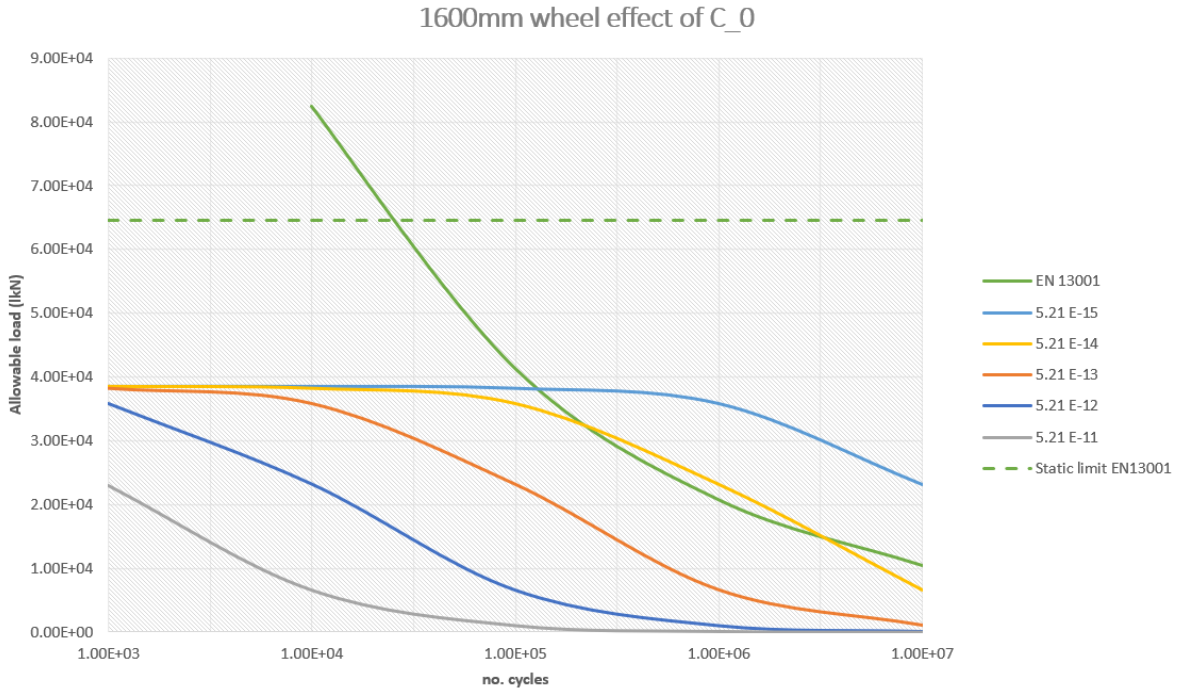

Figure 4.13: Results of varying the value of the intercept constant on the allowed load

Cycles	Load (kN)				
-	C_0 = 5.21 E-11	C_0 = 5.21 E-12	C_0 = 5.21 E-13	C_0 = 5.21 E-14	C_0 = 5.21 E-15
1000	2.30E+04	3.58E+04	3.83E+04	3.86E+04	3.86E+04
10000	6.60E+03	2.32E+04	3.59E+04	3.83E+04	3.86E+04
100000	1.04E+03	6.60E+03	2.32E+04	3.59E+04	3.83E+04
1000000	1.26E+02	1.04E+03	6.60E+03	2.32E+04	3.59E+04
10000000	1.40E+01	1.27E+02	1.04E+03	6.60E+03	2.32E+04

Table 4.9: Resulting values of changing the intercept constant C_0

The results are very different from the previously shown results. Due to the factor change in C_0, the crack growth rate da/dN also changes by a factor of 10, which therefore results in a shift in life expectancy, which is also a factor of 10. This is clearly visible in table 4.9, where an increase in cycles by a factor of 10 results in the same allowed load when C_0 is decreased by a factor of 10.

4.6. Comparing to Experimental Data

The previous sections defined and illustrated four different methods of calculating the allowable fatigue load for steel wheels. Although analysis shown in section 4.4 gives an indication which methods might be more realistic than others, it is very important to compare the results of the model to experimental data for both validation and to indicate which model is closest to reality. Unfortunately, not a lot of experimental data could be found in literature of fatigue on steel wheels. The data that is found will be covered in this section.

4.6.1. Paper: "Effects of Wheel Materials on Wear and Fatigue Damage Behaviors of Wheels/Rails" [40]

As the name suggests, this paper focuses on wear and fatigue damage, and the various effects that occur. The experiment used in this paper uses a cylinder of which the geometry is known, with the maximum contact pressure set to a constant value of 1.100 Mpa. Using the known geometry and the known maximum contact pressure, the load used can be calculated. The experiment tests a number of different heat treatments, but the resulting figures show signs of pitting for most of the wheel/rail contact at 200.000 cycles. This indicates that cracks have grown to the surface of the material. Comparing this data point to the calculation methods results in the following figure:

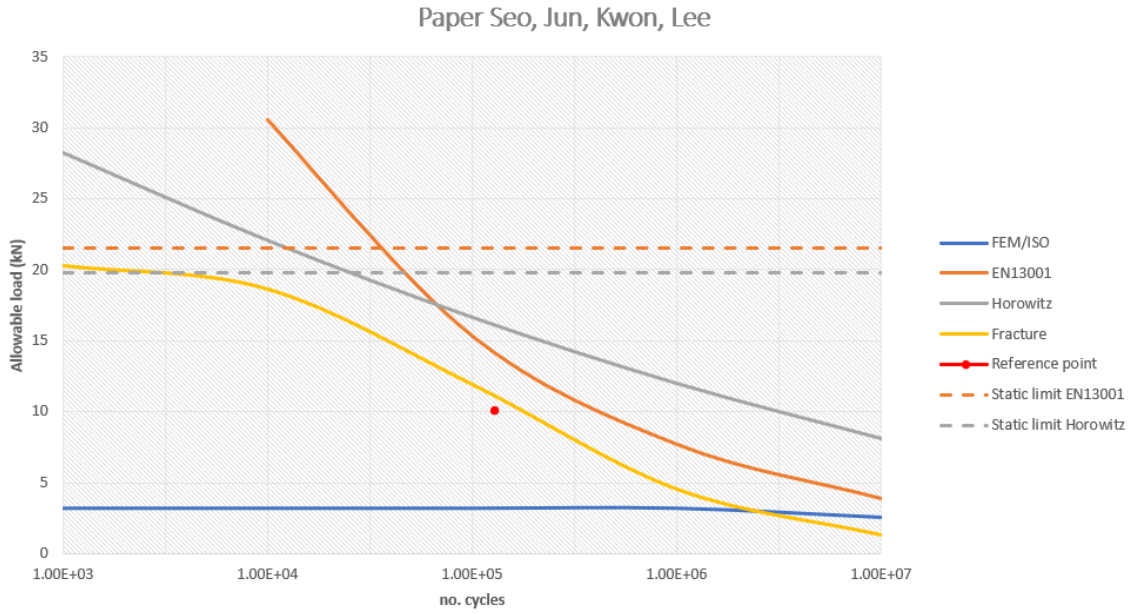

Figure 4.14: Comparing the experimental data point to the calculation methods

The data point shows a result close to the calculation methods. Since the methods have comparable results for cycle numbers higher then 100.000 cycles, this data point is used as a validation. The data point does not indicate which method is more realistic.

4.6.2. HiTeAM Project [41]

This project contains endurance measurements of cylindrical rollers carried out at Huisman. The test setup contains four rollers brought under a specified load of 121.5 metric tons. Damage was inspected at several numbers of cycles, in order to determine the amount of wear and deformations. The material is researched, but although it is assumed cracks are present in the rollers, they could not be seen during microscopic research. This can be due to the fact that the crack faces are closed, and the magnification is not sufficient. Therefore, the failure criterion determined by the EN 13001 standard will be used. A wheel or rail is considered failed at a radial deformation of 0.02% of the wheel radius. Using this criterion, and the test data provided by Huisman, the number of cycles until failure can be approximated. Since the rollers had a diameter of 70 mm, the maximum allowed deformation is 0.014 mm. According to the test data provided by Huisman, no significant wear was observed during the first inspection at 51.000 cycles cycles. However, at the second inspection, which was at 138.000 cycles, the maximum wear averaged for the the four cylinders tested is 0.0175 mm, which is more then the allowed wear. This indicates that the failure criteria are met somewhere

between 51.000 and 138.000 cycles. The resulting data point, which is illustrates as a bar, is compared to the calculation methods in figure 4.15.

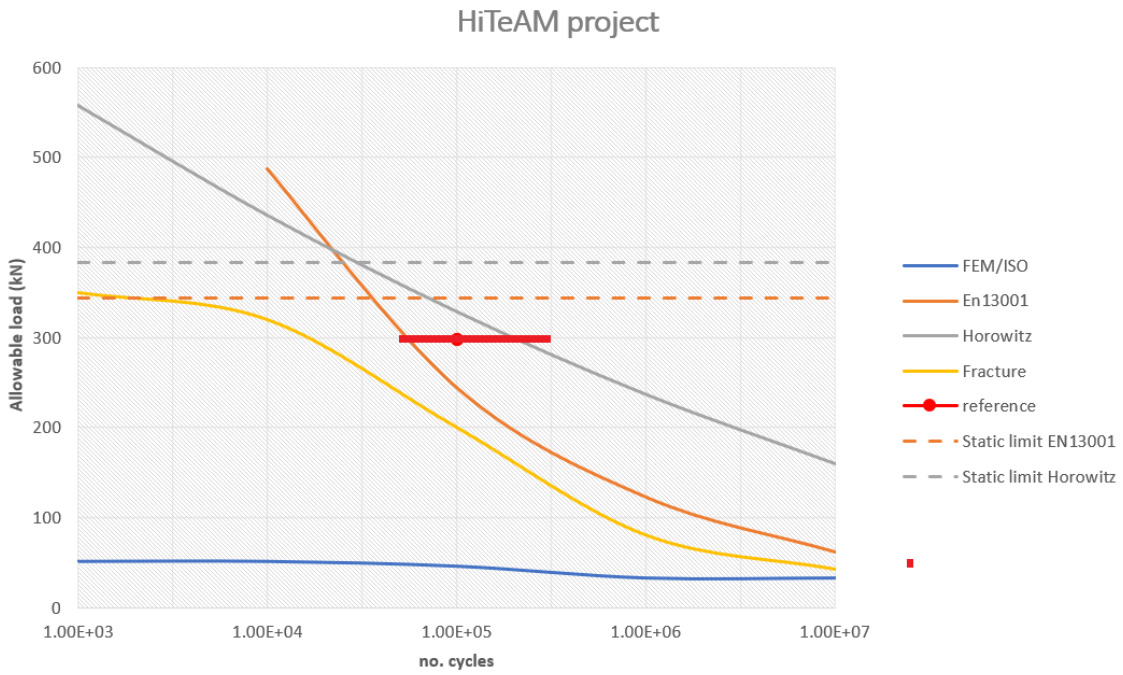

Figure 4.15: Comparing the experimental data point to the calculation methods

Just as the previous data point, the resulting data point is close to the calculation methods. Again, the differences between the different methods are small at cycle numbers of 100.000 and higher. Therefore, this data point does not indicate which method is better then others. It does, however, show that lifetime calculations as function of wear show comparable results to lifetime calculations as a function of crack growth, which is interesting.

4.6.3. Thesis S. Song [42]

A previously written thesis on the topic of fatigue on steel wheels was performed by S. Song, which compared the results for Hertzian stresses to an FEM analysis, and used damage mechanics to calculate remaining lifetime of the wheel. The test setup used three cylindrical rollers with a diameter of 70 mm and a length of 70 mm under a load of 1500 kN [42]. A crack along the surface of the raceway, which was used in calculating damage. According to Song, the damage accumulation rate under these stress conditions increases rapidly at 10^3 cycles, as seen in figure 4.16.

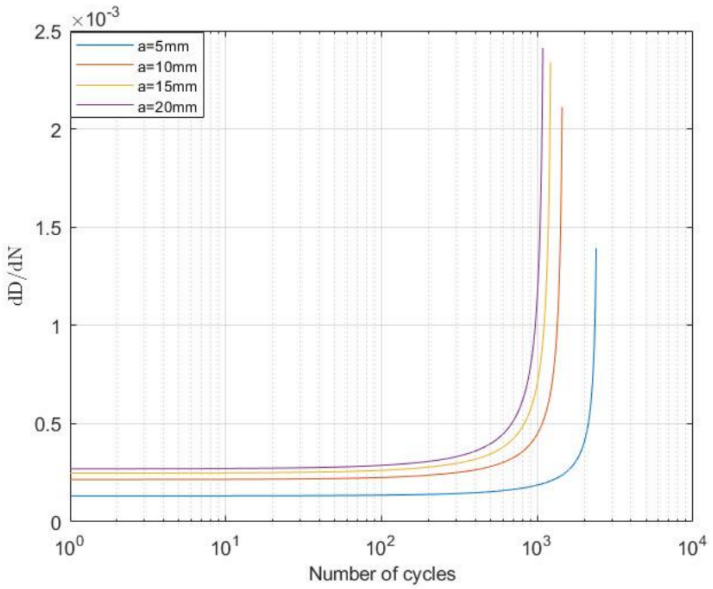

Figure 4.16: Damage accumulation rate for different crack sizes according to Song [42]

This data results in a data point at 10^3 cycles, which is very useful in determining which method is more accurate then others. The resulting data point is compared to the calculation methods in figure 4.17.

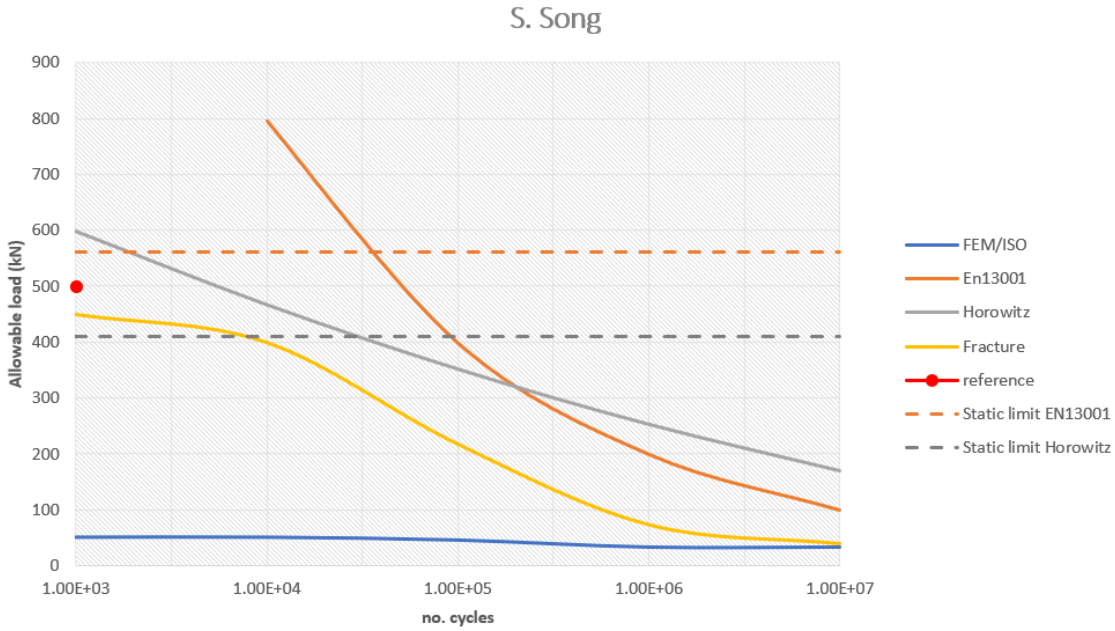

Figure 4.17: Comparing the experimental data point to the calculation methods and the static limits

The data point is slightly higher then the allowed static load according to the Horowitz method, and

slightly lower then the allowed static load according to EN 13001.

The resulting data points indicate that the EN13001 and the Horowitz method are not realistic for low number of cycles (<20000). This is due to the static limit of the wheel/rail, which is also calculated by the same fabrication standards. The FEM/ISO method is also not realistic for low numbers of cycles, since it shows values which are a lot lower then the experimental data points have shown. The fracture mechanics approach shows a realistic trend, but it is very important to have the correct values for the input parameters in order to have a good lifetime prediction.

5

Conclusion and Recommendations

This chapter will conclude the thesis by answering the research questions stated in the introduction, and by making recommendations for improvement and further research.

5.1. Research Question

The research question of this thesis is defined as:

What is the maximum allowable load on steel wheels as a function of number of cycles used for a range between 10^3 *and* 10^7 *cycles? How do these values differ from the calculation standards and which method is most realistic?*

The sub-questions defined in the introduction will be answered in this section.

1. How can the allowable load on steel wheels as a function of lifetime be calculated using fracture mechanics?

In order to use fracture mechanics to calculate the allowed load as a function of lifetime, the stresses resulting from the contact between wheel and rail must be calculated. This is done using the Hertz contact theory. This uses a set of equations to calculate the stresses at surface and sub-surface levels. Since the wheel/rail contact is loaded under compression, the main mode of fatigue will be mode II, which indicates that failure is caused by sub-surface shear stresses resulting from the contact. This is confirmed by failure data from Huisman, which indicates crack initiation at sub-surface level.

Fracture mechanics uses the stress intensity factor, which for mode II is calculated using:

$$K_{II} = Y\tau_{max}\sqrt{\pi a} \tag{5.1}$$

Where a is the crack size and Y is the geometry factor. The maximum shear stress τ_{max} is calculated using Hertz contact theory, and has an angle of 45°with respect to the normal stress (which is perpendicular to the contact surface), as shown by Mohr's circle. This equation does not take any frictional effects into account.

Since the crack is also loaded under compression, frictional effects have to be taken into account. The remaining normal load as function of depth can be calculated, and the depth of maximum shear is known using Hertz contact theory. This, combined with the friction coefficient, results in the following equation for the effective shear stress:

$$\sigma_{se} = \tau_{max} - \sigma_{c2} * k\ sin^2(\theta) \tag{5.2}$$

The effective shear stress will be used to calculate the stress intensity factor.

The stress intensity factor will be used to calculate crack growth. Crack growth can be calculated using differ-

ent equations, of which the Paris' equation will be used in this thesis:

$$\frac{da}{dN} = C(\Delta K)^n \tag{5.3}$$

Here, ΔK is the stress intensity range: $\Delta K = K_{max} - K_{min}$, C and n are the Paris' equation coefficients. This crack growth will be used to calculate the lifetime using the following steps:

1. Calculate K_{max}.
2. If $K_{max} \geq K_c$, the wheel/rail is considered failed and the simulation is stopped. If not, the simulation continues.
3. Calculate stress range and stress intensity range assuming constant amplitude: $\Delta K = K_{max} - K_{min}$.
4. Use crack growth equations to calculate the crack growth rate da/dN.
5. Implement a cycle step size to calculate incremental crack growth.
6. Calculate new crack size and new current total cumber of cycles:

$$a_{i+1} = a_i + \Delta a \qquad N_{i+1} = N_i + \Delta N$$

7. Use the new crack size for the next iteration of the simulation, until the failure condition is met. At this point, the number of cycles until failure N_f is the current number of cycles N_i, and the critical crack size a_c is the current crack size a_i.

2. What are the methods currently used for calculating the maximum allowable load capacity according to the standards?

The three main important standards used by Huisman are:

- EM 1.001 b4 / ISO 16881-1, which is one method used by two standards
- EN 13001-3-3 standard, which is currently the preferred method used by Huisman
- Horowitz, which used to be the preferred method used by Huisman

The FEM/ISO method uses straightforward equations and limited number of inputs, which makes it an easy method to use. Disadvantages are that the limited input parameters create a simplified grasp of the problem, and the fact that the allowed load is calculated using discrete steps, not a continuous formulation. The method is also limited to wheel diameters below 1250 mm, and ultimate strengths higher then 500 N/mm^2/

The EN 13001-3-3 method uses more input parameters then the FEM/ISO method, resulting in more specific and detailed description of the problem. It is also useful for life expectancy calculations. The range in which it can be used is limited:

- $r_k > 5 * min(b_r; b_w)$, in which case the contact is considered a point contact
- $r_k > 200 * min(b_r; b_w)$, in which case the contact is considered a line contact

If the geometry does not meet these requirements, the EN 13001-3-3 method can not be used.

The Horowitz method uses the Hertz stress to calculate the maximum contact pressure, which is then used to calculate the allowed number of cycles for a specific load. It used to be the preferred method used by Huisman, before the EN13001 method was preferred.

Calculations for all three methods are described in chapter 3. Also, the differences in the approaches for Static load, fatigue load and hardening depth are discussed for all three methods.

3. How can the different methods be modeled and compared?

The four different methods are implemented in an analytical model using Excel VBA, which allow for a comparison between the different method in the form of a graph. Explanation of input and output parameters for this model are explained in chapter 4. The wheel/rail contact can also be modeled using an FEA model in order to verify stresses and contact types.

4. How do the results of the fracture mechanics calculations compare to the calculations using methods according to standards, and how to determine which method is most realistic?

The results show many different trends and values, as shown for the 1600 mm wheel in figure 5.1.

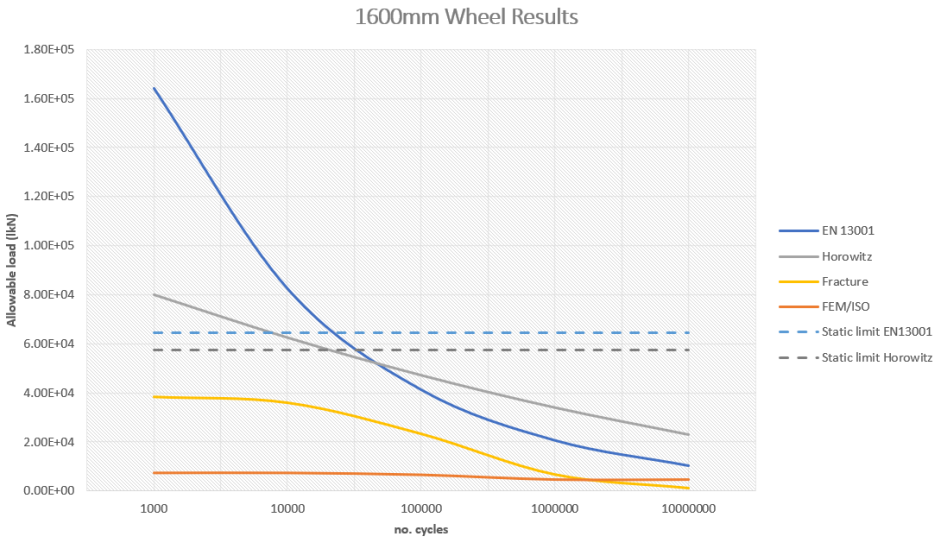

Figure 5.1: Results for all methods plotted for the 1600 mm wheel with static limits included

The FEM/ISO method shows results which do not change much for different cycle numbers, and shows values which are much lower then for all the other methods. The EN13001 method shows an increased rate for lower cycle numbers, while the Horowitz methods has a smaller increase at lower cycle numbers.

The fracture mechanics method shows a different trend than all other methods, by showing a less steep trend at lower cycle numbers then the Horowitz and EN13001 methods. It is to be noted that the input parameters for the fracture mechanics method can have large effects on the results, as shown in the parametric research in section 4.5. The EN13001 and Horowitz method have static limits, as explained in chapter 2, which intersect their fatigue calculation, as shown in figure 5.1. This indicates that the Horowitz and EN13001 method are dependent on both fatigue and static load calculations. This is supported by a simulation provided by S. Song, which show a failure data point located close to the static limits at 1000 cycles [42].

To conclude

Fracture mechanics can be a viable method for calculating the lifetime of wheel/rail contact under specified loads. It is, however, very important that the input parameters for this method are well known, since the output values can change a lot when changing the input parameters.

The EN13001 and Horowitz method showed that their fatigue calculations are not realistic for cycle numbers below 20000 due to their static limit. This is supported by the simulation provided by S. Song [42].

The FEM/ISO method shows results which are much lower then the values presented by the other methods, experimental data supports the expectation that these values are too low, and therefore unrealistic. Due to the simplicity of the calculations for this methods, these results were to be expected.

5.2. Recommendations

5.2.1. Assumptions for Fracture mechanics

During the use of fracture mechanics, assumptions had to be made in order to determine the crack growth rate and the life time of the part. One assumption that has been made is the geometry factor $Y = 1$ independent of the angle. Although the assumptions made for this to be true are accurate, a more detailed use of the geometry factor can be obtained using a detailed FEM analysis or failure data obtained by experiments for certain crack geometries.

The initial crack size a_0 is the maximum original defect size of the material at the beginning of its lifetime, tested with nondestructive testing. If the initial crack size is smaller then the sensitivity of the measuring equipment, the crack size can not be detected, and is therefore assumed to be the size of the measurement sensitivity [31] [14]. Although this is a necessary assumption in order to guarantee a safe choice of initial crack size, it does not actually describe the maximum defect size. If possible, more sensitive equipment can be used to find an actual maximum defect size, which will be smaller than the previously assumed size. This can increase the expected lifetime of a part, and therefore result in possibly more efficient design.

5.2.2. Experimental data

Chapter 4 showed experimental data to validate the calculation methods, and to provide a prediction on which method is realistic. The data used for this prediction is very limited, and might therefore not be enough to give a clear indication of which value is correct. In order to specify which method is more realistic and specify input parameters for fracture mechanics calculations, more data is required. If more experimental data is available, possibly in the form of a graph as the methods have shown in the figures used in this thesis, the material parameters for the fracture mechanics can be specified. These parameters can then be used for other wheel/rail geometries to predict the lifetime or allowed load.

Bibliography

[1] Huisman. *Delivering step changing solutions*. 2021. URL: https://www.huismanequipment.com/en/about_huisman.

[2] L. Hatcher G. Lucas. "Introduction to Standards and Specifications for Design in Mechanics or Strength of Materials". In: (2000). URL: https://sites.esm.psu.edu/courses/emch13d/design/design-tech/standards/specs_8.pdf.

[3] Huisman. "SP-EWI-27380-104-334: Wheels and Rails". In: (2018).

[4] U. Olofsson R. Lewis. *Wheel–Rail Interface Handbook*. Sawston, England: Woodhead Publishing, 2009. URL: https://www.sciencedirect.com/book/9781845694128/wheel-rail-interface-handbook.

[5] H. Hertz. *Ueber die Berührung fester elastischer Körper*. Berlin: De Gruyter, 1882. URL: https://doi.org/10.1515/9783112342404-004.

[6] D. Zhu Q. J. Wang. "Hertz Theory: Contact of Ellipsoidal Surfaces". In: *Encyclopedia of Tribology*. Boston, MA: Springer, 2013. URL: https://doi.org/10.1007/978-0-387-92897-5_493.

[7] Tribonet. *Hertzian contact equations for elliptical, spherical and cylindrical contacts*. 2017. URL: https://www.tribonet.org/wiki/hertz-equations-for-elliptical-spherical-and-cylindrical-contacts/.

[8] Engineering Notes. *Hertzian Contact Stress*. URL: https://www.engineeringnotes.org/solid-mechanics/hertzian-contact-stress/.

[9] F. Cianetti et al. "On the Evaluation of Surface Fatigue Strength of a Stainless-Steel Aeronautical Component". In: (2019). URL: https://www.mdpi.com/2075-4701/9/4/455/htm.

[10] E. Kabo A. Ekberg B. Akesson. "Wheel/rail rolling contact fatigue – Probe, predict, prevent". In: *Wear* 314 (2014), pp. 2–12. URL: https://doi.org/10.1016/j.wear.2013.12.004.

[11] A.M.S. Asih A. Kapoor I. Salehi. "Rolling Contact Fatigue (RCF)". In: *Encyclopedia of Tribology*. Boston, MA: Springer, 2013. URL: https://doi.org/10.1007/978-0-387-92897-5_287.

[12] A.F. Bower. "The Influence of Crack Face Friction and Trapped Fluid on Surface Initiated Rolling Contact Fatigue Cracks". In: *Journal of Tribology* 110(4), (1988), pp. 704–711. URL: https://doi.org/10.1115/1.3261717.

[13] Reza Masoudi Nejad et al. "Stress Intensity Factors Evaluation for Rolling Contact Fatigue Cracks in Rails". In: *Tribology Transactions* 60 (July 2017), pp. 645–652. DOI: 10.1080/10402004.2016.1197351.

[14] MechaniCalc. *Fracture Mechanics*. 2014. URL: https://mechanicalc.com/reference/fracture-mechanics#stress-intensity-factor.

[15] Dr.ir. P.J.G. Schreurs. *Fracture Mechanics*. 2012. URL: https://pdf4pro.com/view/fracture-mechanics-materials-technology-354e5a.html.

[16] G. C. Sih. *Handbook of stress-intensity factors: Stress-intensity factor solutions and formulas for reference*. 3rd ed. Bethlehem, Pa: Lehigh University, Institute of Fracture and Solid Mechanics, 1973.

[17] P. H. Melville. "Fracture Mechanics of Brittle Materials in Compression". In: *International Journal of Fracture* 13 (1977), pp. 532–534. URL: https://link.springer.com/content/pdf/10.1007/BF00034257.pdf.

[18] P. Isaksson. "On Crack Growth under Compressive Stresses". PhD thesis. Lulea University of Technology, 2001. URL: http://www.diva-portal.org/smash/get/diva2:999283/FULLTEXT01.pdf.

[19] G. C. Sih, P. C. Paris, and F. Erdogan. "Crack-Tip, Stress-Intensity Factors for Plane Extension and Plate Bending Problems". In: *Journal of Applied Mechanics* 29.2 (June 1962), pp. 306–312. ISSN: 0021-8936. DOI: 10.1115/1.3640546. URL: https://doi.org/10.1115/1.3640546.

[20] AmesWeb. *Hertzian Contact Stress Formulas*. URL: https://amesweb.info/HertzianContact/HertzianContactCalculationSteps.aspx.

[21] S.G. Kim M. Culpepper. "Contact Mechanics". In: *Principles and techniques for desiging precision machines*, pp. 417–426. URL: https://ocw.mit.edu/courses/mechanical-engineering/2-76-multi-scale-system-design-fall-2004/readings/lec12cont_read.pdf.

[22] MechaniCalc. *Fatigue Crack Growth*. 2014. URL: https://mechanicalc.com/reference/fatigue-crack-growth.

[23] Perez N. "Fatigue Crack Growth. In: Fracture Mechanics". In: *Fracture Mechanics*. 2nd ed. Switzerland: Springer, 2017, pp. 327–372. URL: https://doi.org/10.1007/978-3-319-24999-5_9.

[24] F. Erdogan P. Paris. "A Critical Analysis of Crack Propagation Laws". In: *Journal of Basic Engineering* 85.4 (1963), pp. 528–533. URL: https://doi.org/10.1115/1.3656900.

[25] Cortie M. B. "On the Correlation Between the C and m in the Paris Equation for Fatigue Crack Propagation". In: *Engineering Fracture Mechanics* 30.1 (1988), pp. 49–58. URL: https://doi.org/10.1016/0013-7944(88)90254-8.

[26] The British Standards Institution. "BS 7910: Guide to methods for assessing the acceptability of flaws in metallic structures". In: (2015).

[27] D. Roylance. "Fatigue". PhD thesis. Massachusetts Institute of Technology, 2001. URL: https://ocw.mit.edu/courses/materials-science-and-engineering/3-11-mechanics-of-materials-fall-1999/modules/MIT3_11F99_fatigue.pdf.

[28] J. He Q. Wang X. Li. "A Simple Fatigue Life Prediction Algorithm Using the Modified NASGRO Equation". In: *Mathematical Problems in Engineering* 2016 (2016), p. 8. URL: https://doi.org/10.1155/2016/4298507.

[29] M. A. Meggiolaro. "On the dominant role of crack closure on fatigue crack growth modeling". In: *International Journal of Fatigue* 25 (2003), pp. 843–854. URL: http://meggi.usuarios.rdc.puc-rio.br/paper/R05_IJF03_On_the_dominant_role.pdf.

[30] H.P. Gänser J. Maierhofer R. Pippan. "Modified NASGRO equation for physically short cracks". In: *International Journal of Fatigue* 59 (2014), pp. 200–207. URL: https://doi.org/10.1016/j.ijfatigue.2013.08.019.

[31] X. Liu H. Wang. "Numerical method for estimating fatigue crack initiation size using elastic–plastic fracture mechanics method". In: *Applied Mathematical Modelling* 73 (2019), pp. 365–377. URL: https://doi.org/10.1016/j.apm.2019.04.010.

[32] Satyendra. *Material hardness and hardness testing*. 2016. URL: https://www.ispatguru.com/material-hardness-and-hardness-testing/#:~:text=Material%5C%20hardness%5C%20is%5C%20the%5C%20property,scratching%5C%2C%5C%20abrasion%5C%2C%5C%20or%5C%20cutting..

[33] The Editors of Encyclopaedia Britannica. *Surface hardening*. 2016. URL: https://www.britannica.com/technology/surface-hardening.

[34] G.E. Totten J. Dossett. "Introduction to Surface Hardening of Steels". In: *ASM Handbook*. 4th ed. A S M International, 2013. URL: https://www.asminternational.org/documents/10192/22533690/5344G_Sample_BuyNow.pdf/96e9ae44-b6a1-420c-abf5-ee32a98280d5.

[35] CEN. "EN 13001 - Cranes - General design - Part 3-3: Limit states and proof of competence of wheel/rail contacts". In: (2014).

[36] Federation Europeenne de la Manutention. "FEM 1.001 b4 - Rules for the Design of Hoisting Appliances". In: (1998).

[37] International Organisation of Standardisation. "ISO 16881-1 - Cranes-Design calculation for rail wheels and associated trolley track supporting structure". In: (2003).

[38] A. Horowitz. "Ontwerp en berekening van contraforme contacten". In: (1972).

[39] D. Radaj. "Fracture mechanics approach for assessment of fatigue strength of seam welded joints". In: *Design and Analysis of Fatigue Resistant Welded Structures*. Sawston, England: Woodhead Publishing, 1990, pp. 277–298. URL: https://doi.org/10.1533/9781845698751.277.

[40] Hyun-kyu Jun & Chan-woo Lee Jung-won Seo Seok-jin Kwon. “Effects of Wheel Materials on Wear and Fatigue Damage Behaviors of Wheels/Rails”. In: *Tribology Transactions* 62.4 (2019), pp. 635–649. URL: https://doi.org/10.1080/10402004.2019.1588446.

[41] Huisman. “HiTeam Endurance Test”. In: (2018).

[42] S. Song. “Feasibility of locally-coupled elasto-plastic damage modeling for remaining life prediction of low-speed damaged roller bearings under heavy loading condition”. PhD thesis. Delft University of Technology, 2021.

Appendices

A

Model visualisation

A.1. FEM/ISO model sheet

Geometry		Wheel	Rail	
Diameter	D	300	-	mm
Width	b	150	60	mm
Radius edge	r	0	0	mm
Flange running wheel?	-	no	-	-
Wheel rotation speed	v	100	-	RPM
Spectrum factor	k_c	1	-	-
Material		Wheel	Rail	
		42CrMo4	StE690	
Elastic Modulus	E	210000	210000	Mpa
Yield stress	σy	500	650	Mpa
Ultimate strength	σu	750	760	Mpa
Brinell-Hardness	HB	300	257	Mpa
Demanded no. rotations until failure	10000000			

Figure A.1: Input parameters for FEM/ISO

Calculated values			
Equivalent Diameter	D_eq	300	mm
Effective width	b_eff	60	mm
Equivalent elastic modulus	E_m	210000	Mpa
Limiting pressure	P_L	6.5	MPa
Spectrum class		L4	-
Total duration of use	T(h)	1666.666667	h
Utilization class		T4	-
	Factors further influence		
	c1	0.82	
	c2	0.9	

Figure A.2: Calculated values for FEM/ISO

Allowable static load	F_static	222.3	kN
Allowable fatigue load	F_fatigue	86.346	kN

Figure A.3: Resulting allowed static and fatigue loads for FEM/ISO

A.2. EN 13001 model sheet

Geometry		Wheel	Rail	
Diameter	D	300	-	
Width	b	150	60	
Radius edge	r	0	0	
Wheel curvature radius	rk	1500	0	
Flange running wheel?		no		
Force spectrum factor	k_c	1	-	
Wheel alignment		Self-aligning mounting		
Material		**Wheel**	**Rail**	
		42CrMo4	StE690	
Elastic Modulus	E	210000	210000	Mpa
Yield stress	σy	500	650	Mpa
Ultimate strength	σu	750	760	Mpa
Brinell-Hardness	HB	300	240	Mpa
Surface hardness	HB	530	240	Mpa
Hardening depth	-	5	-	mm
Factors of further influence				
Abrasive particles? (yes or no)	-	no		
Total skew angle	α	0.00445		
Demanded no. rotations / roll-overs until failure	10000000			

Figure A.4: Input parameters for EN 13001

Calculated values				
Equivalent Diameter	D_eq	300		mm
Effective width	b_eff	60		mm
Equivalent elastic modulus	E_m	210000		MPa
Ratio of r_k to b_eff	ratio	25		
Contact type EN13001	Point contact			
		Wheel	Rail	
Hardening factor static	A_s	2100	1680	MPa
Hardening factor fatigue	A_f	900	720	Mpa
Reference contact force	f_u	198.4858239	127.0309	kN
Reference rolling contacts	v_c	1.5625		-
Contact history parameter	S_c	1.5625		
Traveling distance	L	9424.777961		
Tolerance class	Tc	3		
Factors of further influence				
	Static (f_i)	Fatigue (f_fi)		
f1	1	1		
f2	1	-		
f3	-	1		
f4	-	1		
Factors of further infulence	f_f	1		

Figure A.5: Calculated values for EN 13001

		Wheel	Rail	
Allowable static load	F_static	982.4045827	628.7389	kN
Allowable fatigue load	F_fatigue	157.8304524	101.0115	kN

Figure A.6: Resulting allowed static and fatigue loads for EN 13001

A.3. Horowitz model sheet

Geometry		Wheel	Rail
Diameter	D	300	-
Width	b	150	60
Radius edge	r	0	0
Wheel curvature radius	rk	1500	0
Flange running wheel?		no	
Force spectrum factor	k_c	1	-
Wheel alignment		Self-aligning mounting	
Material		**Wheel**	**Rail**
		42CrMo4	StE690
Elastic Modulus	E	210000	210000
Yield stress	σy	500	650
Ultimate strength	σu	750	760
Brinell-Hardness	HB	300	257
Surface hardness	HB	530	257
Hardening depth	mm	5	-
Factors of further influence			
Abrasive particles? (yes or no)		no	
Total skew angle	α	0.00445	
Load for fatigue	900	kN	

Figure A.7: Input parameters for the Horowitz model

Calculated values		
Equivalent Diameter	D_eq	300
Effective width	b_eff	60
Equivalent elastic modulus	E_m	210000
Ratio of r_k to b_eff	ratio	25
Contact type EN13001	Point contact	
Equivalent static rotations	N_static	21074.38894
Hertz stress	σ_H	1915.058876
Traveling distance	L	2584.564433
Tolerance class	Tc	3
Factors of further influence		
	Static (f_i)	Fatigue (f_fi)
f1	1	1
f2	1	-
f3	-	1
f4	-	1

Figure A.8: Calculated values for the Horowitz model

		Wheel	Rail	
Allowable static load	F_static	1788.301318	420.489547	kN
No. Rotations until failure	N_i	2742308.035		

Figure A.9: Resulting allowed static and fatigue loads for Horowitz

A.4. Hertz model sheet

Material		Wheel	Rail					
		42CrMo4	StE690					
Elastic Modulus	E	210000	210000	Mpa				
Poisson ratio	v	0.3	0.3	MPa				
Yield stress	σy	500	650	Mpa				
Ultimate strength	σu	750	760	Mpa				
Brinell-Hardness	HB	300	257	Mpa				
Surface hardness	HB	530	257	Mpa				
Hardening depth	-	5	-	mm				
Geometry								
Contact type		Ellipsoid on plane			Input load	F	100	kN
Wheel radius x	R1x	300	mm					
Wheel radius y	R1y	1500	mm					
Rail radius x	R2x	1500	mm	These values are automatically				
Rail radius y	R2y	1500	mm	ignored if body 2 is plane				

Figure A.10: Input parameters of Hertzian contact model

Calculated values						
Wheel radius x	R1x	1500				
Wheel radius y	R1y	150				
Rail radius x	R2x	1E+99				
Rail radius y	R2y	1E+99				
Effective radius	R_eff	136.3636364	mm			
Effective x radius	R_x	1500	mm			
Effective y radius	R_y	150	mm			
Reduced elastic property	E'	230769.2308	Mpa			
lambda	λ	0.1	-			
kappa	κ	0.222636671	-			
m	m	0.950432913	-			
E(m)	E(m)	1.057533233	-			
alpha	α	0.531198633	-			
Beta	β	2.38594402	-			
Minor contact axis	b_e	2.984037368	mm	Ellipticity	K_e	0.222636671
Major contact axis	a_e	13.40317101	mm	Depth of max shear	z/a	0.162242452
Mean pressure	P_mean	795.862994	Mpa			
Max pressure	P_max	1193.794491	MPa			
Depth of max shear	δ̄	2.174563332	mm			

Figure A.11: Calculated values for the Hertz model

A.5. Fracture mechanics model sheet

Input parameters				
Geometry factor	Y	1	-	
Friction coefficient	k	0.78	-	
Initital crack size	a_0	0.1	mm	
Step size	ΔN	1000	cycles	
Minimum stress	σ_min	0	Mpa	
Paris law exponent	n	3	-	is 3 for steel (british standards)
Intercept constant	C_0	5.21E-13	-	is 5.21x10e-13 for steel in marine environment (british standards)
Walker constant	γ	0	-	
Threshold K	ΔK_th	50	MPa	
Fracture toughness	K_c	100	MPa	
NASGRO coefficient p	p	0	-	
NASGRO coefficient q	q	0	-	
Newman crack closure	f	0	-	

Figure A.12: Input parameters for the Fracture mechanics model

				shear max	min
Calculated values (initial crack)				382.0142371	0
Maximum stress	σ_max	1193.794491	Mpa	Effective shear max	min
Critical angle	θ_0	0.908370033	rad	122.469877	0
Angle of max stress int.	θ_max	0.454185016	rad	K_max	K_min
Max stress intensity factor	K_max	68.64425848		68.64425848	0
Min stress intensity factor	K_min	0			
Stress intensity range	ΔK	68.64425848			
Stress ratio	R	0			
Remaining normal stress in depth	σ_c2	665.4983593			

Figure A.13: Calculated values for the Fracture mechanics model

Paris equation			
no. Cycles until failure	Calculate		372000
Walker equation			
no. Cycles until failure	Calculate		372000
NASGRO equation			
no. Cycles until failure	Calculate		372000

Figure A.14: Resulting values for lifetime, for all three equations, with calculation button for loop

Step	Crack size	K_max	K_min	ΔK	Growth rate
0	0.1	68.64425848	0	68.64426	1.6852E-07
1000	0.10016852	68.70207364	0	68.70207	1.68946E-07
2000	0.100337465	68.75998621	0	68.75999	1.69373E-07
3000	0.100506839	68.81799644	0	68.818	1.69802E-07
4000	0.100676641	68.87610457	0	68.8761	1.70233E-07
5000	0.100846874	68.93431085	0	68.93431	1.70665E-07
6000	0.101017539	68.99261553	0	68.99262	1.71098E-07
7000	0.101188637	69.05101886	0	69.05102	1.71533E-07
8000	0.10136017	69.10952109	0	69.10952	1.71969E-07
9000	0.10153214	69.16812247	0	69.16812	1.72407E-07
10000	0.101704547	69.22682325	0	69.22682	1.72847E-07
11000	0.101877394	69.28562369	0	69.28562	1.73287E-07
12000	0.102050681	69.34452404	0	69.34452	1.7373E-07
13000	0.102224411	69.40352455	0	69.40352	1.74174E-07
14000	0.102398584	69.46262548	0	69.46263	1.74619E-07
15000	0.102573203	69.52182709	0	69.52183	1.75066E-07
16000	0.102748269	69.58112964	0	69.58113	1.75514E-07
17000	0.102923783	69.64053338	0	69.64053	1.75964E-07

Figure A.15: Example of calculation loop (Paris equation is used). The loop continues off-screen, until K_{max} reaches K_c.

B

Wheel Example Images

B.1. Monopile Gripper X Skid 1600mm Wheel

Figure B.1: Wheels during construction of the equipment

B.2. DMPT Top Drive 300mm Bogie Wheel

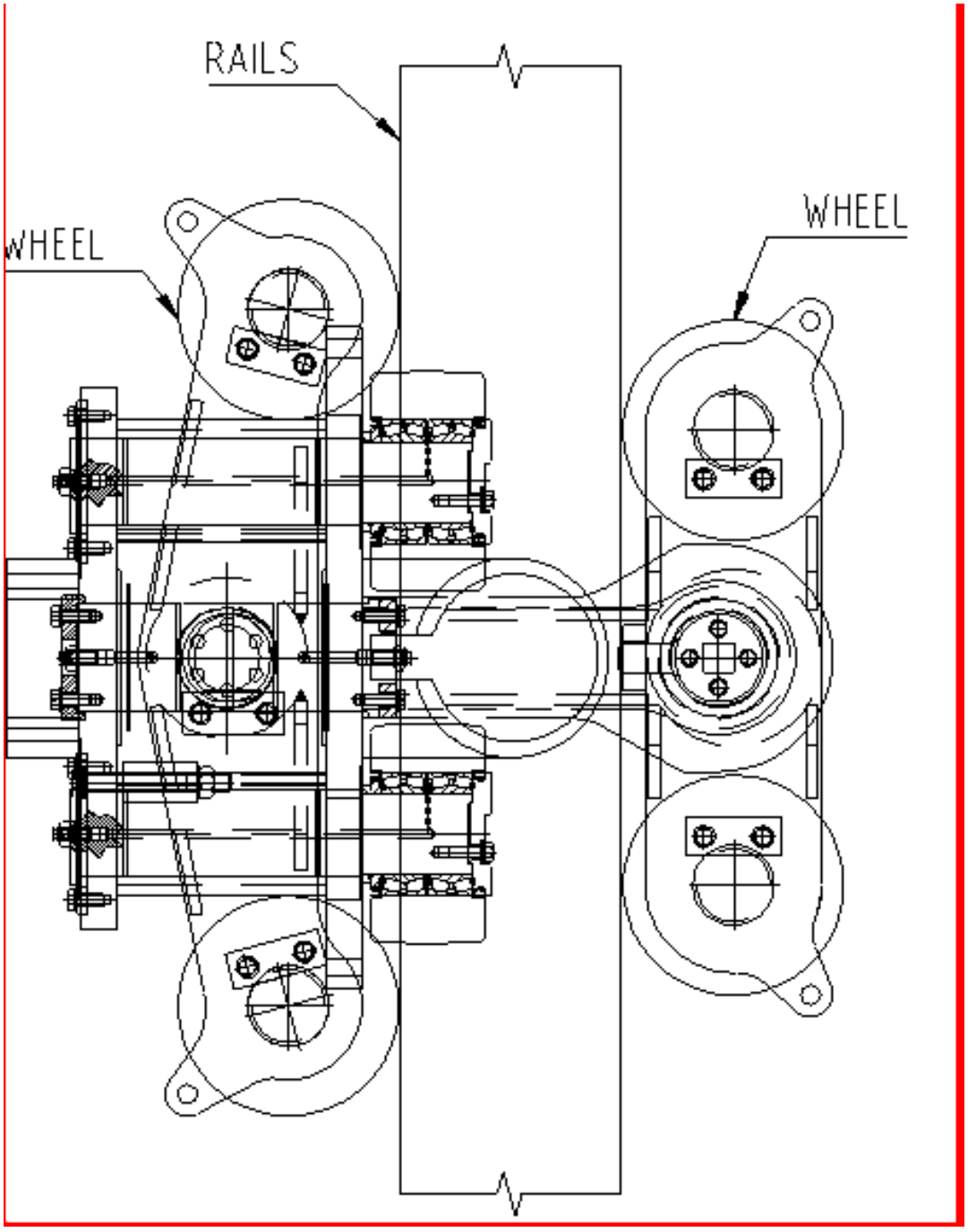

Figure B.2: Technical drawing of the bogie setup